International Journal of Modern Physics B
(2026) 2650132 (39 pages)
© World Scientific Publishing Company
DOI: 10.1142/S0217979226501328

World Scientific
www.worldscientific.com

Dynamic magnetic hysteresis in molecular-based magnetic systems (iii): Application of the path probability method to the mixed-spin (3, 7/2) blume–capel ising model

Mustafa Gençaslan [*,§] and Ahmet Dervişoğlu [†,‡]

[*]*Physics Department, Erciyes University, 38039 Kayseri, Türkiye*

[†]*Department of Astronomy and Space Sciences, Atatürk University, Faculty of Science, Erzurum 25050, Türkiye*

[‡]*Türkiye National Observatories, DAG, Erzurum 25050, Türkiye*

[§]*gaslan@erciyes.edu.tr*

Received 12 September 2025
Revised 4 March 2026
Accepted 12 March 2026
Published 14 May 2026

This study investigates the dynamic hysteresis properties of a mixed-spin (3, 7/2) Blume–Capel Ising system (BCIS) on a square lattice, utilizing the path probability method (PPM) under a time-dependent external magnetic field. The research highlights the critical role of external conditions and intrinsic material parameters in defining the hysteresis characteristics, including coercive fields and remanent magnetization. Unlike previous studies, which either ignored or applied a constant magnetic field, our approach incorporates a sinusoidal magnetic field, enabling a comprehensive analysis of the kinetic magnetic properties. The results demonstrate significant variations in the dynamic magnetic response, revealing insights into temperature dependency, oscillation frequency and rate constants, thus contributing to a better understanding of molecular-based magnetic materials.

Keywords: Dynamic magnetic hysteresis loops; magnetic materials; mixed-spin (3, 7/2) Blume–Capel Ising systems; anisotropy; path probability method; multiple hysteresis loops.

PACS numbers: 75.10.Hk, 75.60.Ej, 05.70.Ln, 75.30.Kz

1. Introduction

The field of molecular-based magnetic materials continues to be a major focus of research due to its profound implications for technological innovation in areas such as high-density data storage, spintronics and quantum computing.[1–5] To realize the full potential of these materials, a fundamental understanding of their dynamic magnetic response is essential. Key characteristics like the coercive field (CF) and remanent magnetization (RM), which are derived from magnetic hysteresis loops,

[§]Corresponding author.

are critical metrics for performance and reliability in magnetic devices.[6,7] Therefore, a systematic investigation into how these properties evolve under diverse external conditions and intrinsic material parameters is paramount for designing next-generation functional systems.

A variety of theoretical frameworks have been developed to model the dynamic behavior of Ising-type spin systems. Widely used approaches include mean-field theory (MFT),[8–11] effective-field theory (EFT),[12–15] and Monte Carlo (MC) simulations.[16–23] These methods have provided significant insights into the dynamic phase transitions and hysteresis phenomena in mixed-spin systems, especially on simple lattice geometries under oscillating magnetic fields. However, these conventional techniques have well-known limitations. While MFT and EFT offer analytical simplicity, they often rely on approximations that neglect important spin correlations and may fail to capture complex kinetic effects. Conversely, MC simulations, though powerful, are computationally demanding, particularly when modeling systems under continuous driving fields or when incorporating microscopic kinetic parameters.

To address these limitations, the path probability method (PPM), first proposed by Kikuchi,[24] has emerged as a robust theoretical tool. The PPM provides a self-consistent framework for treating thermodynamic and kinetic processes on an equal footing, making it uniquely suitable for studying nonequilibrium phenomena. By formulating time-dependent master equations for the probabilities of microscopic configurations, the PPM allows for a direct investigation of a system's evolution under dynamic external stimuli. A key advantage of the PPM is its intrinsic ability to incorporate kinetic rate constants (k_2). These constants can be directly mapped onto physical processes, such as spin-flip relaxation dynamics or the cooling rate (i.e., "wheel speed") in rapid solidification techniques used in materials science.[25–28]

When defining the Hamiltonian for a system used to determine the kinetic magnetic properties of molecular-based magnetic materials, either a pure-spin Ising system or a mixed-spin Ising system can be employed. The Blume–Capel (BC) or Blume–Emery–Griffiths (BEG) approaches are most commonly preferred for constructing the Hamiltonian. This Hamiltonian expression typically includes a single-ion anisotropy parameter, which is specific to the crystal lattice chosen for the system, and an external magnetic field parameter, if applicable. The external magnetic field can be constant or time-dependent (e.g., sinusoidal), though the latter choice can slightly increase computational complexity.

Limited research exists in the literature concerning the mixed-spin (3, 7/2) Blume–Capel Ising system (BCIS), which is utilized in our current study. The few existing studies, while employing various crystal lattices, have either used a constant external magnetic field or omitted it entirely. Furthermore, the Hamiltonian expression in these works exclusively adopts the BC approach, a preference also maintained in our present study. Arejdal *et al.*[29] investigated the magnetic properties of a mixed-spin (3, 7/2) BCIS for a magnetic nanoparticle system on a dendrimer structure under a constant external magnetic field using MC simulations.

They obtained the ground-state phase diagrams of the system and examined the temperature dependence of sublattice and total magnetizations, as well as hysteresis curve behaviors. Similarly, Arejdal *et al.*[30] applied the same methods to determine the stable phases and hysteresis curve behaviors of the system. Masrour and Jabar[31] studied the magnetic properties of double-layered graphene nanoribbons on an armchair lattice using a mixed-spin (3, 7/2) BCIS under a constant magnetic field, employing MC simulations. They obtained the ground-state phase diagrams, magnetizations for various system parameters and hysteresis curves. Bouda *et al.*[32] utilized a mixed-spin (3, 7/2) BC ferrimagnetic Ising model on a square lattice without an external magnetic field to investigate the compensation temperature behavior of the system using MC simulations. They obtained ground-state phase diagrams and the temperature dependence of magnetizations for different crystal lattice parameters. Abed and Mohamad[33,34] employed the molecular MFT to obtain the compensation temperature behavior and the temperature dependence of magnetizations for a mixed-spin (3, 7/2) BC ferrimagnetic Ising model on square and cubic lattices, respectively, without an external magnetic field. Karimou *et al.*[35] used MFT to determine the compensation temperatures for various crystal lattice parameters of a mixed-spin (3, 7/2) BC ferrimagnetic Ising model on a square lattice without an external magnetic field.

As can be observed, studies investigating the dynamic magnetic properties of magnetic materials using the mixed-spin (3, 7/2) BCIS are exceptionally scarce. A significant reason for this scarcity is that the analytical and numerical calculations (which generate numerous systems of nonlinear differential equations) required to explain the kinetic properties of magnetic materials using high-spin mixed-spin Ising systems are considerably more time-consuming. Among the existing studies, the external magnetic field, which has a significant impact on dynamic magnetic properties, has either been entirely omitted[33–35] or treated as constant.[29–32] In contrast, our current work will not only apply an external magnetic field to the system but also ensure that this field is time-dependent. Furthermore, the PPM, which will be employed in this study, has not been used previously for the mixed-spin (3, 7/2) BCIS. This method will enable the investigation of the kinetic magnetic properties (hysteresis curves, phase transition temperatures, compensation temperatures, dynamic phase diagrams) of molecular-based magnetic materials using a mixed-spin (3, 7/2) BCIS on a square lattice under a time-dependent external magnetic field, for both ferrimagnetic and antiferrimagnetic states. PPM avoids stochastic noise inherent to MC, goes beyond mean-field Glauber by introducing independent kinetic constants for rotational/translational relaxations, and affords deterministic integration of the coupled kinetics with direct experimental mapping of k_2 (wheel-speed). In addition to PPM-based studies, recent investigations using MC, mean-field/effective-field with Glauber-type dynamics, and stochastic φ^4-model frameworks[36–40] further broaden the kinetic modeling landscape for dynamic hysteresis in magnetic systems.

One of the unique contributions of this study is the application of an external magnetic field that varies with time to the system. Another key originality of this work is the utilization of the PPM for the mixed-spin (3, 7/2) BCIS, a method highly suitable for examining the kinetic magnetic properties of molecular-based magnetic materials. A further significant original contribution is that the results obtained with PPM, benefiting from the advantage of the rate constant coefficient yielded by this method, can be compared with experimental results obtained by researchers employing rapid solidification techniques. Mixed high-spin configurations such as (3, 7/2) are representative of Fe^{3+}–Nd^{3+} or Mn^{3+}–Gd^{3+} pairs in molecular magnets and melt-spun rare-earth alloys.

Very recently, we have investigated the dynamic hysteresis loop behaviors of molecule-based magnetic materials by applying the PPM method to a high-spin mixed-spin BCIS on a square or hexagonal lattice under an oscillating external magnetic field.[41–43] In this study, we focus on the square lattice — a geometry highly relevant for modeling two-dimensional materials. We will conduct a thorough comparative analysis of the mixed-spin (3, 7/2) model for both ferrimagnetic ($J > 0$) and antiferrimagnetic ($J < 0$) interactions. Our goal is to leverage the unique capabilities of the PPM to elucidate how the interplay of temperature (T), crystal field (D), field frequency (ω) and the kinetic rate constant (k_2) dictates the dynamic magnetic response in this higher-order spin system. This advantage of PPM in reproducing rate-dependent loop areas and multi-loop features has been cross-checked against MC and dynamic-mean-field results reported in Refs. 43–45. In contrast to previous mixed-spin studies with static/zero fields, our work integrates a sinusoidally varying field together with explicit kinetic rate constants, enabling frequency- and rate-dependent hysteresis analysis. This work constitutes the third installment of our systematic investigation of dynamic magnetic hysteresis in molecular-based mixed-spin systems. While previous studies focused on the hexagonal lattice geometry, the current contribution examines the square lattice case to explore lattice-dependent dynamic effects.

The remainder of this paper is organized as follows. Section 2 details the theoretical model and the PPM formulation. Section 3 will present the numerical results and discussion. Finally, Sec. 4 summarizes our main findings and outlines future research directions.

2. Method and Formulation

This study investigates the dynamic magnetic hysteresis curves of molecular-based magnetic materials. It does this by employing a mixed-spin ($\sigma_A = 3, S_B = 7/2$) BCIS on a square lattice, subjected to a sinusoidal external magnetic field. The lattice is two-dimensional with periodic boundary conditions; only nearest-neighbor σ–S exchange is included, each sublattice occupying half of the sites. The PPM, a robust nonequilibrium statistical mechanics approach developed by Kikuchi[24] and extensively applied to dynamic phenomena in cooperative systems for analyzing the time

evolution of the system's dynamic order parameters, is utilized. This section details the theoretical framework, including the system's Hamiltonian, the application of the Blume–Capel model, the formulation of kinetic equations within the PPM using the pair approximation, and the numerical procedures for simulating dynamic hysteresis.

The system under consideration is a two-dimensional square lattice where each lattice site is occupied by an atom with either spin $\sigma^A = 3$ or $S^B = 7/2$. This mixed-spin configuration is chosen to mimic the complex magnetic interactions observed in certain molecular magnets, which often exhibit multiple magnetic sites with varying spin values. We consider a checkerboard-like arrangement on the square lattice, ensuring equal concentrations of A ($\sigma^A = 3$) and B (spin $S^B = 7/2$) sites. The BC model is particularly well-suited for describing systems with single-ion anisotropy (crystal field interactions). The Hamiltonian of the system is given by

$$H = -J \sum_{<ij>} \sigma_i^A S_j^B - D\left[\sum_i (\sigma_i^A)^2 + \sum_j (S_j^B)^2\right] - H\left(\sum_i \sigma_i^A + \sum_j S_j^B\right), \quad (1)$$

where J is the exchange coupling constant between nearest-neighbor spins $\langle ij \rangle$. We consider ferrimagnetic coupling ($J > 0$), and antiferrimagnetic coupling ($J < 0$). The second term addresses single-ion anisotropy, or the crystal field parameter D. Its sign and magnitude dictate the energetic preference for or against nonzero spin states. The final term describes the Zeeman interaction between the spins and the time-dependent magnetic field, which is given by $H = H_0 \sin(\omega t)$. This field is applied to all spins in the system, influencing both A and B sublattices simultaneously. This sinusoidal field drives the system through dynamic hysteresis loops.

The PPM, within the framework of the cluster variation method (CVM),[24] is employed to derive the nonequilibrium kinetic equations governing the time evolution of the system's macroscopic properties. For our mixed-spin (3, 7/2) system on a square lattice, utilizing the pair approximation, the state of the system is described by a set of 13 independent average order parameters. These parameters are derived from the single-site probabilities of finding a spin in a particular state on the A or B sublattices, and the nearest-neighbor pair probabilities between A and B sites.

Specifically, the average order parameters are defined as the probabilities of finding a spin at a given site with a specific spin value, and the probabilities of finding a pair of nearest-neighbor spins with specific values. The state probabilities P_i for sublattice A and P_j for sublattice B are defined as the time-dependent probabilities that spins occupy their respective states. For the spin-3 sublattice A, there are seven allowed spin states ($\sigma = \pm 3, \pm 2, \pm 1, 0$). Conversely, the spin-7/2 sublattice B has eight allowed spin states ($S = \pm 7/2, \pm 5/2, \pm 3/2, \pm 1/2$). This results in a system defined by 15 state probabilities and 13 associated average order parameters, ensuring the closure of the PPM equations under normalization conditions.

The order parameters for the mixed-spin (3, 7/2) BCIS are

For layer A: average magnetization $m^A \equiv \langle \sigma_i^A \rangle$, quadrupole moment $q^A \equiv \langle (\sigma_i^A)^2 \rangle$, octupole moment $r^A \equiv \langle (\sigma_i^A)^3 \rangle$. hexadecapole moment $o^A \equiv \langle (\sigma_i^A)^4 \rangle$,

dotriacontapole moment $p^A \equiv \langle(\sigma_i^A)^5\rangle$, and tetrahexadecapole moment $t^A \equiv \langle(\sigma_i^A)^6\rangle$.

For layer B: average magnetization $m^B \equiv \langle S_j^B\rangle$, quadrupole moment $q^B \equiv \langle(S_j^B)^2\rangle$, octupole moment $r^B \equiv \langle(S_j^B)^3\rangle$, hexadecapole moment $o^B \equiv \langle(S_j^B)^4\rangle$, dotriacontapole moment $p^B \equiv \langle(S_j^B)^5\rangle$, tetrahexadecapole moment $t^B \equiv \langle(S_j^B)^6\rangle$, and octadecosahectapole moment $u^B \equiv \langle(S_j^B)^7\rangle$. We can express these average order parameters as a function of the state probabilities, as follows:

$$m^A = 3P_1^A + 2P_2^A + P_3^A - P_5^A - 2P_6^A - 3P_7^A, \tag{2a}$$

$$q^A = 9P_1^A + 4P_2^A + P_3^A + P_5^A + 4P_6^A + 9P_7^A, \tag{2b}$$

$$r^A = 27P_1^A + 8P_2^A + P_3^A - P_5^A - 8P_6^A - 27P_7^A, \tag{2c}$$

$$o^A = 81P_1^A + 16P_2^A + P_3^A + P_5^A + 16P_6^A + 81P_7^A, \tag{2d}$$

$$p^A = 243P_1^A + 32P_2^A + P_3^A - P_5^A - 32P_6^A - 243P_7^A, \tag{2e}$$

$$t^A = 729P_1^A + 64P_2^A + P_3^A + P_5^A + 64P_6^A + 729P_7^A. \tag{2f}$$

and

$$m^B = \frac{7}{2}P_1^B + \frac{5}{2}P_2^B + \frac{3}{2}P_3^B + \frac{1}{2}P_4^B - \frac{1}{2}P_5^B - \frac{3}{2}P_6^B - \frac{5}{2}P_7^B - \frac{7}{2}P_8^B, \tag{3a}$$

$$q^B = \frac{49}{4}P_1^B + \frac{25}{4}P_2^B + \frac{9}{4}P_3^B + \frac{1}{4}P_4^B + \frac{1}{4}P_5^B + \frac{9}{4}P_6^B + \frac{25}{4}P_7^B + \frac{49}{4}P_8^B, \tag{3b}$$

$$r^B = \frac{343}{8}P_1^B + \frac{125}{8}P_2^B + \frac{27}{8}P_3^B + \frac{1}{8}P_4^B - \frac{1}{8}P_5^B - \frac{27}{8}P_6^B - \frac{125}{8}P_7^B - \frac{343}{8}P_8^B, \tag{3c}$$

$$o^B = \frac{2401}{16}P_1^B + \frac{625}{16}P_2^B + \frac{81}{16}P_3^B + \frac{1}{16}P_4^B + \frac{1}{16}P_5^B + \frac{81}{16}P_6^B + \frac{625}{16}P_7^B + \frac{2401}{16}P_8^B, \tag{3d}$$

$$p^B = \frac{16807}{32}P_1^B + \frac{3125}{32}P_2^B + \frac{243}{32}P_3^B + \frac{1}{32}P_4^B - \frac{1}{32}P_5^B - \frac{243}{32}P_6^B - \frac{3125}{32}P_7^B - \frac{16807}{32}P_8^B, \tag{3e}$$

$$t^B = \frac{117649}{64}P_1^B + \frac{15625}{64}P_2^B + \frac{729}{64}P_3^B + \frac{1}{64}P_4^B + \frac{1}{64}P_5^B + \frac{729}{64}P_6^B + \frac{15625}{64}P_7^B + \frac{117649}{64}P_8^B, \tag{3f}$$

$$u^B = \frac{823543}{128}P_1^B + \frac{78125}{128}P_2^B + \frac{2187}{128}P_3^B + \frac{1}{128}P_4^B - \frac{1}{128}P_5^B - \frac{2187}{128}P_6^B - \frac{78125}{128}P_7^B - \frac{823543}{128}P_8^B. \tag{3g}$$

The state probabilities can be easily expressed in terms of the average order parameters using Eqs. (2)–(3) and the normalization condition. This will be necessary to

obtain the kinetic order parameters. Thus, the state probabilities for layers A and B, respectively, are given by

$$P_1^A = \frac{1}{60}m^A + \frac{1}{180}q^A - \frac{1}{48}r^A - \frac{1}{144}o^A + \frac{1}{240}p^A + \frac{1}{720}t^A, \tag{4a}$$

$$P_2^A = -\frac{3}{20}m^A - \frac{3}{40}q^A + \frac{1}{6}r^A + \frac{1}{12}o^A - \frac{1}{60}p^A - \frac{1}{120}t^A, \tag{4b}$$

$$P_3^A = \frac{3}{4}m^A + \frac{3}{4}q^A - \frac{13}{48}r^A - \frac{13}{48}o^A + \frac{1}{48}p^A + \frac{1}{48}t^A, \tag{4c}$$

$$P_4^A = -\frac{49}{36}q^A + \frac{7}{18}o^A - \frac{1}{36}t^A + 1, \tag{4d}$$

$$P_5^A = -\frac{3}{4}m^A + \frac{3}{4}q^A + \frac{13}{48}r^A - \frac{13}{48}o^A - \frac{1}{48}p^A + \frac{1}{48}t^A, \tag{4e}$$

$$P_6^A = \frac{3}{20}m^A - \frac{3}{40}q^A - \frac{1}{6}r^A + \frac{1}{12}o^A + \frac{1}{60}p^A - \frac{1}{120}t^A, \tag{4f}$$

$$P_7^A = -\frac{1}{60}m^A + \frac{1}{180}q^A + \frac{1}{48}r^A - \frac{1}{144}o^A - \frac{1}{240}p^A + \frac{1}{720}t^A. \tag{4g}$$

and

$$P_1^B = -\frac{5}{7168}m^B + \frac{259}{23040}q^B + \frac{37}{11520}r^B - \frac{7}{1152}o^B - \frac{1}{576}p^B + \frac{1}{1440}t^B + \frac{1}{5040}u^B - \frac{5}{2048}, \tag{5a}$$

$$P_2^B = \frac{49}{5120}m^B - \frac{499}{4608}q^B - \frac{499}{11520}r^B + \frac{59}{1152}o^B + \frac{59}{2880}p^B - \frac{1}{288}t^B - \frac{1}{720}u^B + \frac{49}{2048}, \tag{5b}$$

$$P_3^B = -\frac{245}{3072}m^B + \frac{1299}{2560}q^B + \frac{433}{1280}r^B - \frac{15}{128}o^B - \frac{5}{64}p^B + \frac{1}{160}t^B + \frac{1}{240}u^B - \frac{245}{2048}, \tag{5c}$$

$$P_4^B = \frac{1225}{1024}m^B - \frac{1891}{4608}q^B - \frac{1891}{2304}r^B + \frac{83}{1152}o^B + \frac{83}{576}p^B - \frac{1}{288}t^B - \frac{1}{144}u^B + \frac{1225}{2048}, \tag{5d}$$

$$P_5^B = -\frac{1225}{1024}m^B - \frac{1891}{4608}q^B + \frac{1891}{2304}r^B + \frac{83}{1152}o^B - \frac{83}{576}p^B - \frac{1}{288}t^B + \frac{1}{144}u^B + \frac{1225}{2048}, \tag{5e}$$

$$P_6^B = \frac{245}{3072}m^B + \frac{1299}{2560}q^B - \frac{433}{1280}r^B - \frac{15}{128}o^B + \frac{5}{64}p^B + \frac{1}{160}t^B - \frac{1}{240}u^B - \frac{245}{2048}, \tag{5f}$$

$$P_7^B = -\frac{49}{5120}m^B - \frac{499}{4608}q^B + \frac{499}{11520}r^B + \frac{59}{1152}o^B - \frac{59}{2880}p^B - \frac{1}{288}t^B + \frac{1}{720}u^B + \frac{49}{2048}, \tag{5g}$$

$$P_8^B = \frac{5}{7168}m^B + \frac{259}{23040}q^B - \frac{37}{11520}r^B - \frac{7}{1152}o^B + \frac{1}{576}p^B + \frac{1}{1440}t^B - \frac{1}{5040}u^B - \frac{5}{2048}. \tag{5h}$$

The dynamic equations governing the average order parameters can be derived using the PPM. Kikuchi's seminal work[24] established the fundamental PPM equation, which quantifies the rate of change for state variables:

$$\frac{dP_i}{dt} = \sum_{i \neq j} (\mathrm{X}_{ji} - \mathrm{X}_{ij}). \tag{6}$$

In this expression, X_{ji} signifies the path probability function describing the system's transition from state i to state j. The principle of detailed balance mandates that $\mathrm{X}_{ji} = \mathrm{X}_{ij}$. Our current investigation employs Kikuchi's Recipe II,[24] formulated as

$$\mathrm{X}_{ij} = k_{ij} Z^{-1} P_i \exp\left(-\frac{\beta}{N}\left(\frac{\partial E}{\partial P_j}\right)\right). \tag{7}$$

Here, $\beta = 1/1k_BT$, where k_B is the Boltzmann constant. For all calculations presented in this study, k_B was fixed at 1.0. The terms k_{ij} represent the rate constants, with the condition $k_{ij} = k_{ji}$. A key advantage of the PPM over alternative well-known methodologies is its reliance on three distinct coupling constants (k_1, k_2 and k_3), which are instrumental for studying system dynamics. Specifically, k_1 corresponds to the rate of spin particle insertion or removal during lattice translation. k_2 describes the rate of spin particle reorientation at a fixed site, while k_3 represents the simultaneous translation and rotation of particles. Through the geometric mean condition, k_3 can be expressed as $k_3 = \sqrt{k_1 k_2}$. Given that rotational relaxation times are typically shorter than translational relaxation times in most physical systems, k_2 generally exceeds k_1. In our computations, k_1 was maintained at a constant value of 1.0, while k_2 was varied. The rate constants for layers A and B are provided in Table 1.

The partition function Z for each of the layers A and B is defined as

$$Z^A = \sum_{i=1}^{7} \exp\left[-\frac{\beta}{N}\left(\frac{\partial E}{\partial P_i^A}\right)\right], \quad Z^B = \sum_{j=1}^{8} \exp\left[-\frac{\beta}{N}\left(\frac{\partial E}{\partial P_j^B}\right)\right], \tag{8}$$

where N denotes the number of spin particles and E signifies the system's internal energy. The internal energy can be computed from P_i^A and P_j^B using Eqs. (2)–(3):

$$\frac{E}{N} = -Jm^A m^B - Dq^A - Dq^B - Hm^A - Hm^B. \tag{9}$$

Table 1. The description of rate constants for the layers A and B. k_1 represents spin particle translation, k_2 signifies spin particle rotation at a given site and k_3 denotes simultaneous spin translation and rotation. The geometric mean, k_3 can be expressed as $k_3 = \sqrt{k_1 k_2}$.

Layer A	P_1 (3)	P_2 (2)	P_3 (1)	P_4 (0)	P_5 (-1)	P_6 (-2)	P_7 (-3)
P_1 (3)		k_1	k_1	k_1	k_3	k_3	k_2
P_2 (2)	k_1		k_1	k_1	k_3	k_2	k_3
P_3 (1)	k_1	k_1		k_1	k_2	k_3	k_3
P_4 (0)	k_1	k_1	k_1		k_1	k_1	k_1
P_5 (-1)	k_3	k_3	k_2	k_1		k_1	k_1
P_6 (-2)	k_3	k_2	k_3	k_1	k_1		k_1
P_7 (-3)	k_2	k_3	k_3	k_1	k_1	k_1	

Layer B	P_1 (7/2)	P_2 (5/2)	P_3 (3/2)	P_4	P_5 ($-1/2$)	P_6 ($-3/2$)	P_7 ($-5/2$)	P_8 ($-7/2$)
P_1 (7/2)		k_1	k_1	k_1	k_3	k_3	k_3	k_2
P_2 (5/2)	k_1		k_1	k_1	k_3	k_3	k_2	k_3
P_3 (3/2)	k_1	k_1		k_1	k_3	k_2	k_3	k_3
P_4 (1/2)	k_1	k_1	k_1		k_2	k_3	k_3	k_3
P_5 ($-1/2$)	k_3	k_3	k_3	k_2		k_1	k_1	k_1
P_6 ($-3/2$)	k_3	k_3	k_2	k_3	k_1		k_1	k_1
P_7 ($-5/2$)	k_3	k_2	k_3	k_3	k_1	k_1		k_1
P_8 ($-7/2$)	k_2	k_3	k_3	k_3	k_1	k_1	k_1	

For the mixed-spin $(3, 7/2)$ BCIS, the dynamic magnetic characteristics are primarily captured by two order parameters: m^A and m^B. To ensure the system of equations is closed and solvable, we defined and computed additional order parameters. To maintain focus within the main body of the text, only the dynamic equations for m^A and m^B are presented here, with the remaining equations relegated to the appendix.

The implementation of the PPM proceeds through the following stages: (i) initialization of state probabilities for the A ($\sigma = 3$) and B ($S = 7/2$) sublattices; (ii) evaluation of the corresponding order parameters (m^A, m^B, q^A, q^B, ...); (iii) construction of the coupled kinetic equations using Kikuchi's Recipe II within the PPM framework; and (iv) numerical time integration of these equations with the Adams–Moulton predictor–corrector method to obtain the dynamic magnetizations and hysteresis characteristics.

The dynamic equations are subsequently derived by combining Eqs. (4)–(9). Consequently, the dynamic equation for the average magnetization of layer A is given by

$$\begin{aligned}\Omega \frac{dm^A}{d\xi} = \Bigg\{ \Bigg[\left(\frac{7}{30} k_1 - 3k_2 + \frac{23}{30} k_3 \right) e^b \cosh(a) + \left(\frac{22}{15} k_1 + \frac{6}{5} k_2 - \frac{14}{3} k_3 \right) \\ \times e^{4b} \cosh(2a) + \left(\frac{27}{10} k_1 - \frac{1}{5} k_2 - \frac{9}{2} k_3 \right) e^{9b} \cosh(3a) - 2k_1 \Bigg] m^A \\ + \Bigg[\left(-\frac{467}{180} k_1 + 3k_2 - \frac{73}{180} k_3 \right) e^b \sinh(a)\end{aligned}$$

$$
\begin{aligned}
&+\left(-\frac{178}{45}k_1-\frac{3}{5}k_2+\frac{41}{9}k_3\right)e^{4b}\sinh(2a)\\
&+\left(-\frac{319}{60}k_1+\frac{1}{15}k_2+\frac{21}{4}k_3\right)e^{9b}\sinh(3a)\Bigg]q^A\\
&+\Bigg[\left(-\frac{1}{4}k_1+\frac{13}{12}k_2-\frac{5}{6}k_3\right)e^{b}\cosh(a)+\left(\frac{1}{2}k_1-\frac{4}{3}k_2+\frac{11}{6}k_3\right)\\
&\times e^{4b}\cosh(2a)+\left(-\frac{3}{4}k_1+\frac{1}{2}k_2+\frac{1}{2}k_3\right)e^{9b}\cosh(3a)\Bigg]r^A\\
&+\Bigg[\left(\frac{23}{36}k_1-\frac{13}{12}k_2+\frac{4}{9}k_3\right)e^{b}\sinh(a)+\left(\frac{37}{36}k_1+\frac{2}{3}k_2-\frac{61}{36}k_3\right)\\
&\times e^{4b}\sinh(2a)+\left(\frac{17}{12}k_1-\frac{1}{12}k_2-\frac{4}{3}k_3\right)e^{9b}\sinh(3a)\Bigg]o^A\\
&+\Bigg[\left(\frac{1}{60}k_1-\frac{1}{12}k_2+\frac{1}{15}k_3\right)e^{b}\cosh(a)+\left(\frac{1}{30}k_1+\frac{2}{15}k_2-\frac{1}{6}k_3\right)\\
&\times e^{4b}\cosh(2a)+\frac{1}{20}(k_1-k_2)e^{9b}\cosh(3a)\Bigg]p^A\\
&+\Bigg[\left(-\frac{2}{45}k_1+\frac{1}{12}k_2-\frac{7}{180}k_3\right)e^{b}\sinh(a)+\left(-\frac{13}{180}k_1-\frac{1}{15}k_2+\frac{5}{36}k_3\right)\\
&\times e^{4b}\sinh(2a)+\left(-\frac{1}{10}k_1+\frac{1}{60}k_2+\frac{1}{12}k_3\right)e^{9b}\sinh(3a)\Bigg]t^A\\
&+2k_1(\sinh(a)e^{b}+2\sinh(2a)e^{4b}+3\sinh(3a)e^{9b}\}\\
&/(k(1+2\cosh(a)e^{b}+2\cosh(2a)e^{4b}+2\cosh(3a)e^{9b}))
\end{aligned}
\tag{10a}
$$

and for layer B by

$$
\begin{aligned}
\Omega\frac{dm^B}{d\xi}=\Bigg\{&\Bigg[\left(-\frac{1225}{512}k_2+\frac{3371}{26880}k_1+\frac{14363}{53760}k_3\right)e^{b_4}\cosh(a_4)\\
&+\left(\frac{21291}{8960}k_1-\frac{86997}{17920}k_3+\frac{245}{512}k_2\right)e^{b_3}\cosh(a_3)\\
&+\left(-\frac{49}{512}k_2-\frac{70225}{10752}k_3+\frac{24875}{5376}k_1\right)e^{b_2}\cosh(a_2)\\
&+\left(\frac{26411}{3840}k_1-\frac{68257}{7680}k_3+\frac{5}{512}k_2\right)e^{b_1}\cosh(a_1)\Bigg]m^B\\
&+\Bigg[\left(\frac{16933}{11520}k_3-\frac{1891}{2304}k_2-\frac{3739}{5760}k_1\right)e^{b_4}\sinh(a_4)\\
&+\left(\frac{5519}{2304}k_3-\frac{3739}{5760}k_1+\frac{3897}{1280}k_2\right)e^{b_3}\sinh(a_3)\\
&+\left(-\frac{3739}{5760}k_1+\frac{2217}{1280}k_3-\frac{2495}{2304}k_2\right)e^{b_2}\sinh(a_2)\\
&+\left(\frac{1133}{2304}k_3+\frac{1813}{11520}k_2-\frac{3739}{5760}k_1\right)e^{b_1}\sinh(a_1t)\Bigg]q^B
\end{aligned}
$$

$$
\begin{aligned}
&+\left[\left(\frac{1289}{1152}k_3+\frac{1891}{1152}k_2-\frac{301}{576}k_1\right)e^{b_4}\cosh(a_4)\right.\\
&+\left(\frac{1299}{640}k_2-\frac{301}{192}k_1+\frac{6907}{1920}k_3\right)e^{b_3}\cosh(a_3)\\
&+\left(\frac{499}{1152}k_2+\frac{279}{128}k_3-\frac{1505}{579}k_1\right)e^{b_2}\cosh(a_2)\\
&\left.+\left(\frac{259}{5760}k_2+\frac{21329}{5760}k_3-\frac{2107}{579}k_1\right)e^{b_1}\cosh(a_1)\right]r^B\\
&+\left[\left(\frac{83}{576}k_2+\frac{19}{288}k_1-\frac{121}{576}k_3\right)e^{b_4}\sinh(a_1)\right.\\
&+\left(\frac{19}{288}k_1+\frac{367}{576}k_3-\frac{45}{64}k_2\right)e^{b_3}\sinh(a_3)\\
&+\left(-\frac{37}{64}k_3+\frac{19}{288}k_1+\frac{295}{576}k_2\right)e^{b_2}\sinh(a_2)\\
&\left.+\left(\frac{11}{576}k_3+\frac{19}{288}k_1-\frac{49}{576}k_2\right)e^{b_1}\sinh(a_1)\right]o^B\\
&+\left[\left(\frac{293}{1440}k_3+\frac{61}{720}k_1-\frac{83}{288}k_2\right)e^{b_4}\cosh(a_4)\right.\\
&+\left(\frac{15}{32}k_2+\frac{61}{240}k_1-\frac{347}{480}k_3\right)e^{b_3}\cosh(a_3)\\
&+\left(-\frac{7}{32}k_3+\frac{61}{144}k_1-\frac{59}{288}k_2\right)e^{b_2}\cosh(a_2)\\
&\left.+\left(\frac{427}{720}k_1-\frac{899}{1440}k_3+\frac{7}{288}k_2\right)e^{b_1}\cosh(a_1)\right]p^B\\
&+\left[\left(-\frac{1}{360}k_1+\frac{7}{720}k_3-\frac{1}{144}k_2\right)e^{b_4}\sinh(a_3)\right.\\
&+\left(-\frac{1}{360}k_1-\frac{5}{144}k_3+\frac{3}{80}k_2\right)e^{b_3}\sinh(a_3)\\
&+\left(\frac{3}{80}k_3-\frac{1}{360}k_1-\frac{5}{144}k_2\right)e^{b_2}\sinh(a_2)\\
&\left.+\left(-\frac{1}{144}k_3-\frac{1}{360}k_1+\frac{7}{720_2}\right)e^{b_1}\sinh(a_1)\right]t^B\\
&+\left[\left(-\frac{5}{504}k_3-\frac{1}{252}k_1+\frac{7}{720}k_2\right)e^{b_4}\cosh(a_4)\right.\\
&+\left(-\frac{1}{40}k_2+\frac{31}{840}k_3-\frac{1}{84}k_1\right)e^{b_3}\cosh(a_3)\\
&+\left(\frac{1}{168}k_3-\frac{5}{252}k_1+\frac{1}{72}k_2\right)e^{b_2}\cosh(a_2)\\
&\left.+\left(-\frac{1}{36}k_1+\frac{11}{360}k_3-\frac{1}{360}k_2\right)e^{b_1}\cosh(a_1)\right]u^B\\
&+\left(\frac{1225}{1024}k_2-\frac{363}{1024}k_3+\frac{81}{512}k_1\right)e^{b_4}\sinh(a_4)
\end{aligned}
$$

$$+\left(\frac{593}{512}k_1+\frac{2621}{1024}k_3-\frac{735}{1024}k_2\right)e^{b_3}\sinh(a_3)$$
$$+\left(\frac{1105}{512}k_1+\frac{2665}{1024}k_3+\frac{245}{1024}k_2\right)e^{b_2}\sinh(a_2)$$
$$+\left(\frac{1617}{512}k_1+\frac{3969}{1024}k_3-\frac{35}{1024}k_2\right)e^{b_1}\sinh(a_1)\Bigg\}$$
$$/(2k(\cosh(a_1)e^{b_1}+\cosh(a_2)e^{b_2}+\cosh(a_3)e^{b_3}+\cosh(a_4)e^{b_4}) \quad (11a)$$

where $a=(Jm^B+h)/T,\ b=d/T,\ c=(Jm^A+h)/T,\ a_1=\frac{7}{2}c,\ a_2=\frac{5}{2}c,\ a_3=\frac{3}{2}c,$ $a_4=\frac{1}{2}c,\ b_1=\frac{49}{4}b,\ b_2=\frac{25}{4}b,\ b_3=\frac{9}{4}b,\ b_4=\frac{1}{4}b,\ h=H/z,\ d=D/z,\ T=(\beta z)^{-1},\ z=4$ and $\Omega=\omega/k,\ k=k_1k_2,\ k_3=\sqrt{k_1k_2},\ \xi=\omega t$. We nondimensionalize by setting $J=1$ and $k_B=1.0$; hence $d\equiv D/(zJ)$, $h\equiv H(zJ)$ and $T\equiv 1/(\beta zJ)$. For brevity, we write $d=D/z$, $h=H/z$ and $T\equiv 1/(\beta z)$ with $J=1$ understood.

To thoroughly examine the system's dynamic magnetic behavior, our analysis focuses on the time-dependent magnetizations m^A and m^B of the A and B sublattices. After the transient regime disappears, these magnetizations become periodic with the same period as the external oscillating magnetic field. Therefore, the dynamic order parameters of the system are defined as the time-averaged magnetizations of the sublattices over one full cycle of the oscillating field and can be written as

$$M^{A,B}=\frac{1}{2\pi}\int_0^{2\pi}m^{A,B}(\omega t)dt. \quad (12)$$

Here, M^A and M^B denote the dynamic order parameters of the A and B sublattices, respectively.

The area of the dynamic magnetic hysteresis loop for both A and B layers can be expressed as[46]

$$A=-\oint m^{A,B}(t)dH=H_0\omega\oint m^{A,B}(t)\sin(\omega t)dt. \quad (13)$$

This quantity corresponds to the area enclosed by the hysteresis loop and represents the energy loss during one cycle of the oscillating magnetic field. Furthermore, the total magnetization, denoted as M^T, is defined as the average of M^A and M^B: $M^T=(M^A+M^B)/2$.

The numerical calculations for this study involved a comprehensive set of 13 nonlinear differential equations with 13 unknown variables. These equations, specifically Eqs. (10a), (11a), (A.10b)–(A.10f) and (A.11b)–(A.11g), were derived, and the corresponding code for the numerical calculation program was generated using the MAPLE computer algebra system. The dynamic equations were solved numerically using the Adams–Moulton predictor–corrector method. After the transient regime disappears and the system reaches a periodic stationary state, the dynamic order parameters defined in Eq. (12) were obtained by averaging the periodic

magnetizations over one full cycle using the Romberg integration method. This computational process was executed using Python and C++, incorporating the predefined system parameters and initial values. The subsequent section will present and discuss these results in detail.

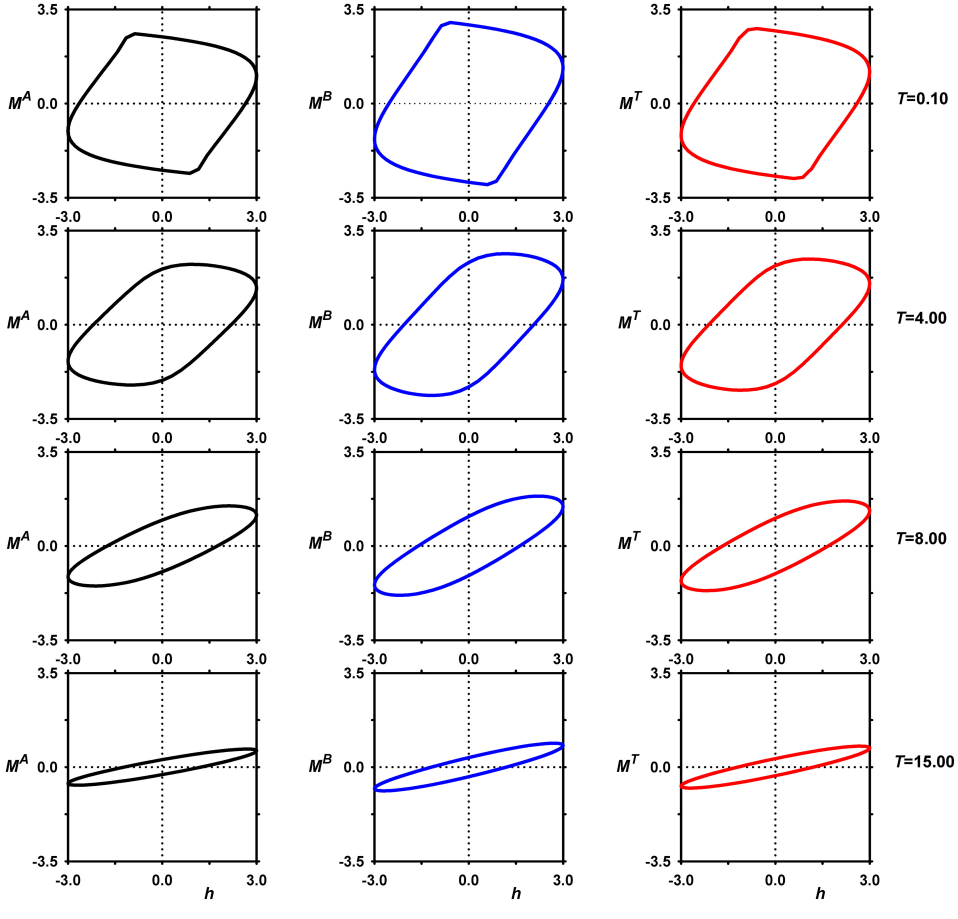
3. Numerical Results and Discussion

We have presented our findings in a total of eight figures, with four figures each for the $J > 0$ and $J < 0$ cases. Each set of four figures includes results for temperature (T), oscillation frequency (ω), reduced single-ion anisotropy (d) and the rate constant (k_2). Each figure consists of two parts: group (a) shows the dynamic hysteresis loop area profiles for magnetizations m^A, m^B and m^T for specific values of the relevant system parameters, while group (b) presents the behavior of the CFs and RMs for the hysteresis loops as a function of the relevant system parameters. In all figures, behaviors related to m^A, m^B and m^T are color-coded; m^A is black, m^B is blue and m^T is red, respectively.

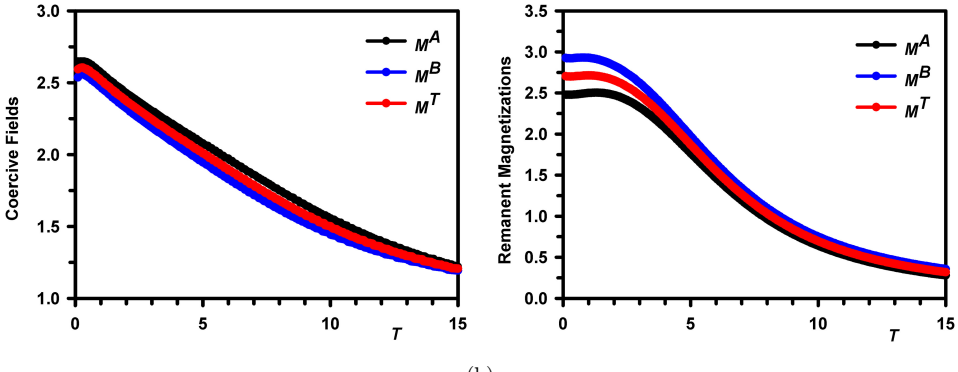
3.1. *Results for J>0 case*

For the ferrimagnetic case ($J > 0$), we first investigated the kinetic hysteresis loop areas of the system as a function of temperature. Figure 1 illustrates the kinetic magnetic hysteresis behaviors obtained from calculations for d =2.0, k_2 =2.0, and $\omega = 1.50\pi$. Looking at Fig. 1(a), which shows results for specific temperature values, it is clear that the kinetic hysteresis loops for m^A, m^B and m^T reach maximum saturation at low temperatures and have a symmetric rectangular shape. As the temperature rises, these loop areas progressively narrow and transform into a symmetric elliptical form. We did not observe any multi-loops during this process. Figure 1(b) presents the CFs and RMs as a function of temperature. Here, the kinetic CF behaviors for m^A, m^B and m^T magnetizations are initially close at low temperatures and then decrease, becoming nearly equal at higher temperatures. Similar trends are seen for the RM, except for differences in saturation points at low temperatures. Shrinking of the kinetic magnetic hysteresis loop areas with increasing temperature and their transformation into a very narrow, symmetric ellipse shape that remains almost unchanged has been reported in theoretical studies on many Ising-type mixed-spin systems[43–45,47–51] and in experimental studies on molecular-based magnetic materials.[52,53]

Figure 2 shows the behavior of the kinetic hysteresis loops depending on the oscillating external magnetic field frequency ω, where $d = 2.0$, $k_2 = 2.0$ and $T = 0.50$ are used. It is important to note that, similar to Fig. 1, the kinetic loop areas reach a maximum saturation point at low temperatures. Likewise, they exhibit a symmetric rectangular shape at low temperatures; however, as the temperature increases, the areas narrow while still retaining their rectangular structure. Another similarity is the absence of multi-loop behavior. The corresponding CFs and RMs for these loop

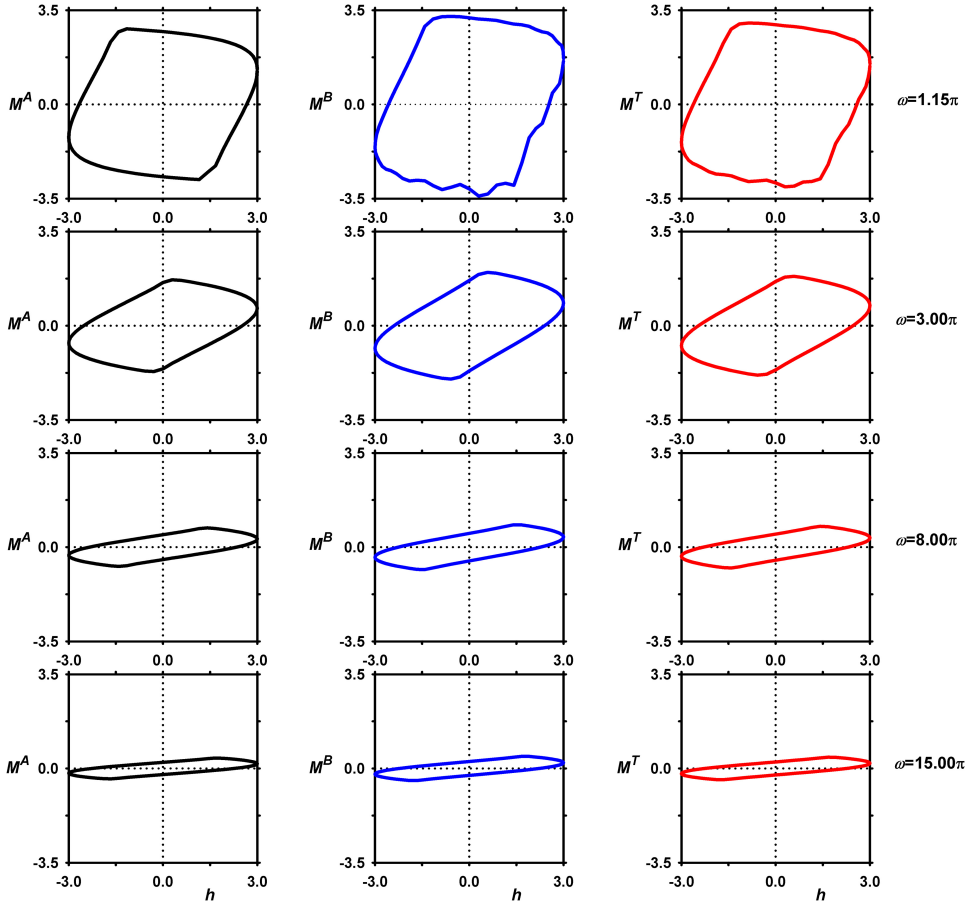


(a)

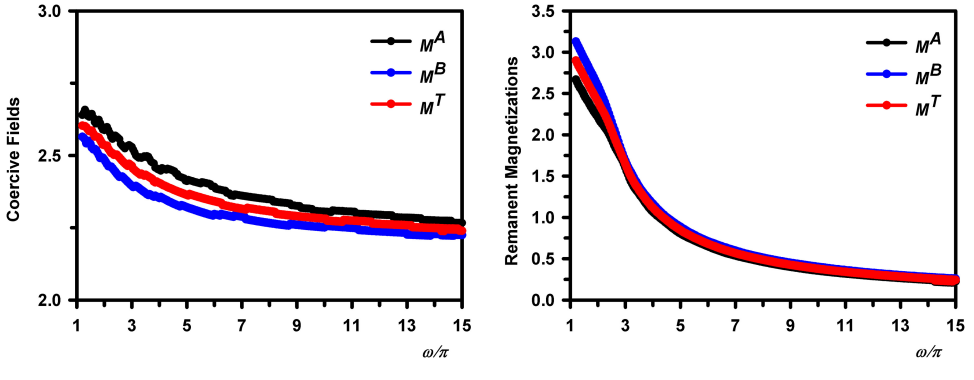


(b)

Fig. 1. (Color online) (a) The KMHLBs of m^A, m^B and m^T for fix $h_0 = 3.00$, $d = 2.0$, $\omega = 1.50\pi$, $k_1 = 1.0$, $k_2 = 2.0$, but various temperature T values. (b) The behaviors of CFs and the RMs as a function of T.



(a)



(b)

Fig. 2. (Color online) (a) The KMHLBs of m^A, m^B and m^T for fix $h_0 = 3.00$, $d = 2.0$, $T = 0.50$, $k_1 = 1.0$, $k_2 = 2.0$, but various frequencies of the oscillating field ω values. (b) The behaviors of CFs and the RMs as a function of ω.

behaviors are shown in Fig. 2(b). The behavior of CFs and RMs obtained as a function of the oscillating external magnetic field frequency is characteristically the same as that obtained as a function of temperature: the areas decrease with increasing frequency. This type of kinetic magnetic hysteresis loop behavior, where multi-loops are not observed and the CFs and RMs are not zero, is encountered in many theoretical studies[44,49,54–57] and experimental studies[58–61] on the kinetic properties of mixed-spin ferrimagnetic Ising spin systems.

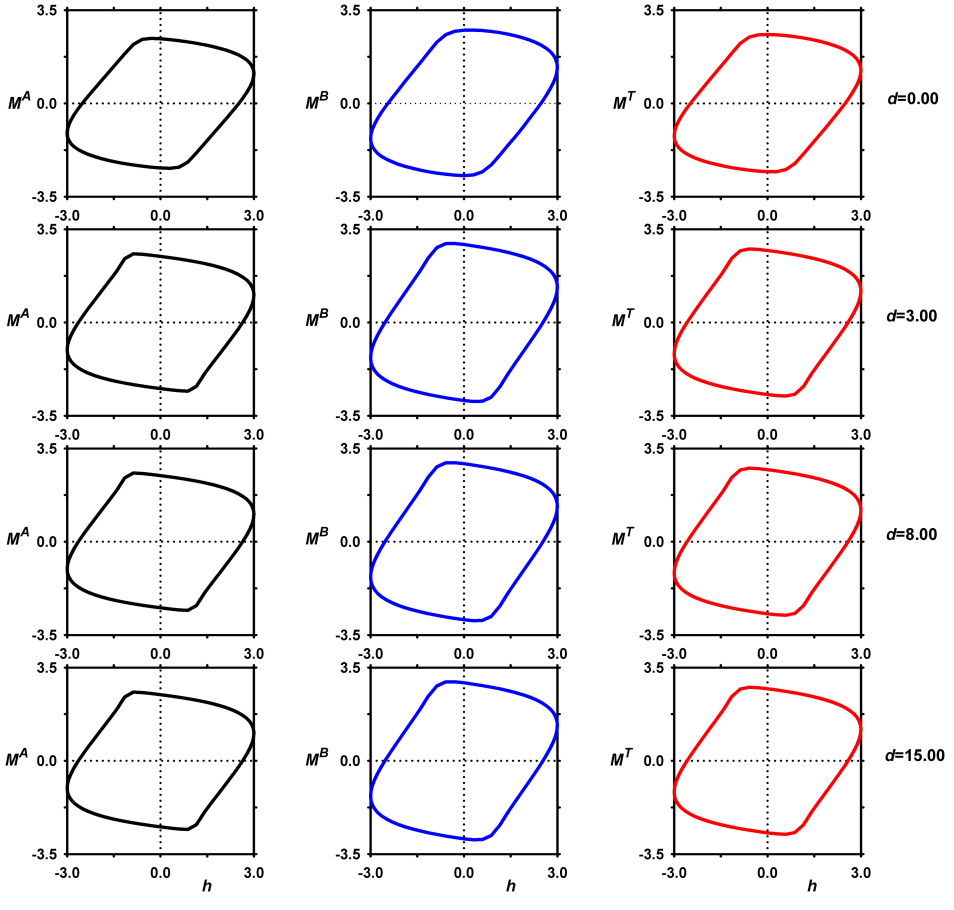
Figure 3 was generated to observe the effect of the reduced crystal main parameter, d, on the kinetic hysteresis curves, where we used $\omega = 1.50\pi$, $k_2 = 2.0$ and $T = 0.50$. We observed that, except for very small values of d, it had little effect on both the kinetic hysteresis curves and the CF and RM curves. Although the initially symmetric rectangular structure for m^A, m^B and m^T changed only slightly, there was almost no effect with increasing d. This situation is clearly seen in Figs. 1(a) and 1(b).

Figure 4 presents the results obtained based on the k_2 rate parameter, one of the most crucial parameters of the PPM. Here $d = 2.0$, $\omega = 6.00\pi$ and $T = 0.50$ were used. At low k_2 values, the kinetic hysteresis curves obtained for m^A, m^B and m^T exhibit narrow, rectangular behaviors. As k_2 increases, the areas of these rectangular curves expand, reaching a maximum saturation point at $k_2 = 7.35$. Beyond this point, no further behavior is observed. Furthermore, because multi-loops do not form from the beginning of k_2, and there is no multi-loop transition, the CF and RM behaviors do not decrease to zero; instead, they reach maximum CF and RM with increasing k_2. The increase in the area of kinetic magnetic hysteresis loops without exhibiting multiple loops, as well as the fact that the area remains unchanged after a specific value of k_2, is in perfect agreement with theoretical studies on mixed-spin ferrimagnetic Ising spin systems[43,44] and with experimental studies, particularly those using the melt-spinning method.[62–65]

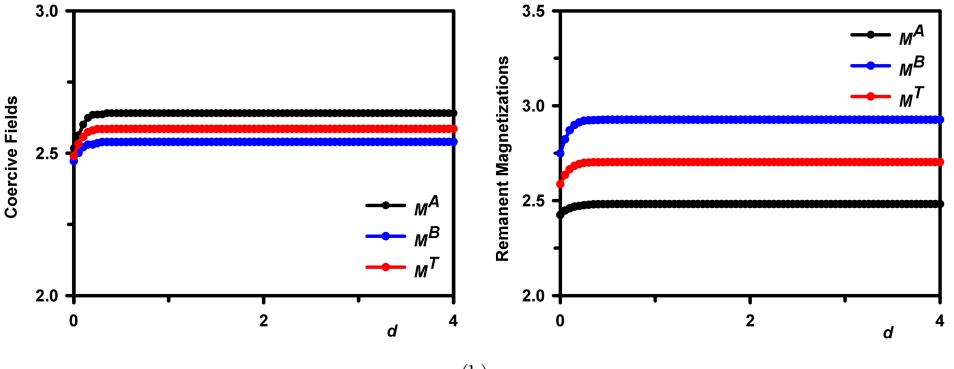
3.2. *Results for J<0 case*

In this antiferrimagnetic state, multiple loops were observed in all the kinetic magnetic hysteresis loops obtained for all system parameters. Their common characteristics are low saturation points and very narrow triple and double loop areas.

Figure 5 shows the kinetic magnetic hysteresis loops as a function of temperature and the corresponding behaviors of CFs and RMs for $d = 2.0$, $k_2 = 2.0$ and $\omega = 3.65\pi$. It is noteworthy that the kinetic magnetic hysteresis loops for magnetizations m_A, m_B and m_T exhibit a narrow-area triple-loop behavior at low temperatures. With increasing temperature, m_B first, then m_T, and subsequently m_A transform into narrow-area double loops. In all three cases, after the kinetic magnetic hysteresis loops convert to double loops, they exhibit a symmetric elliptical behavior with progressively narrowing areas as the temperature increases. This kinetic magnetic hysteresis loop behavior is clearly seen from the CFs and RMs, which start at low temperatures and become zero at $T = 1.70$, 2.70 and 3.65 for m^A, m^T and m^B, respectively, while CFs increase and RMs decrease thereafter. Kinetic magnetic

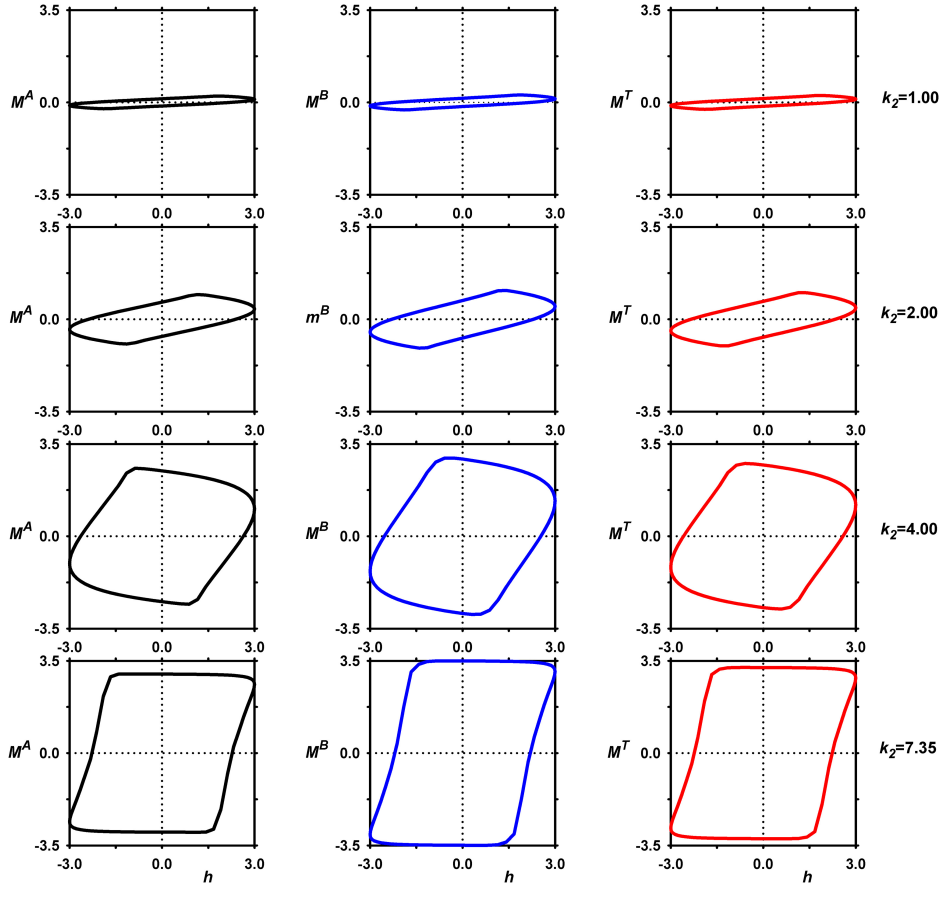


(a)

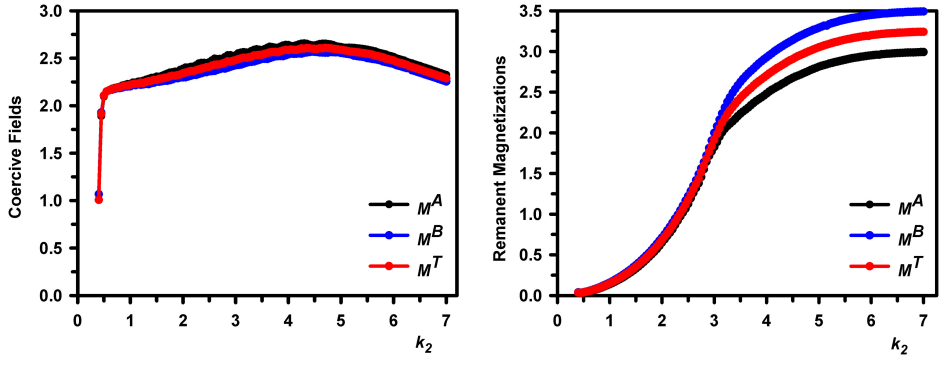


(b)

Fig. 3. (Color online) (a) The DMHLBs of m^A, m^B and m^T for fix $h_0 = 3.00$, $\omega = 1.50\pi$, $T = 0.50$, $k_1 = 1.0$, $k_2 = 2.0$, but various crystal-field interaction d values. (b) The behaviors of CFs and the RMs as a function of d.

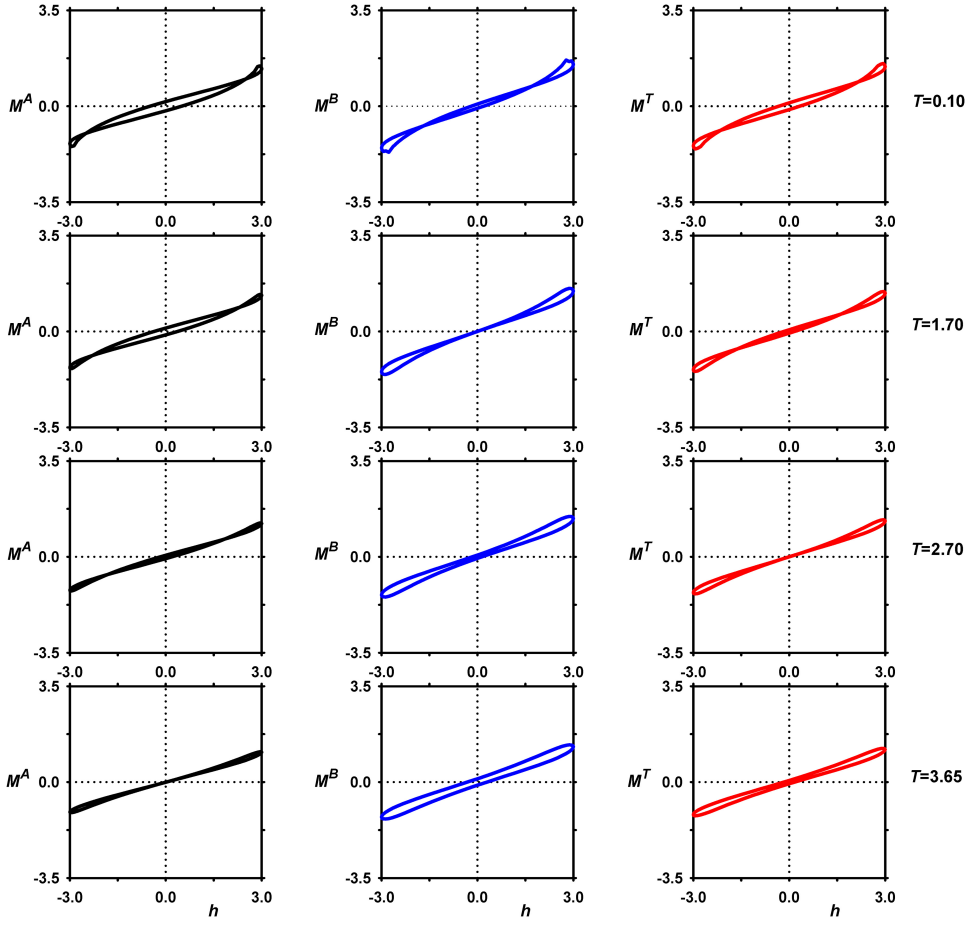


(a)

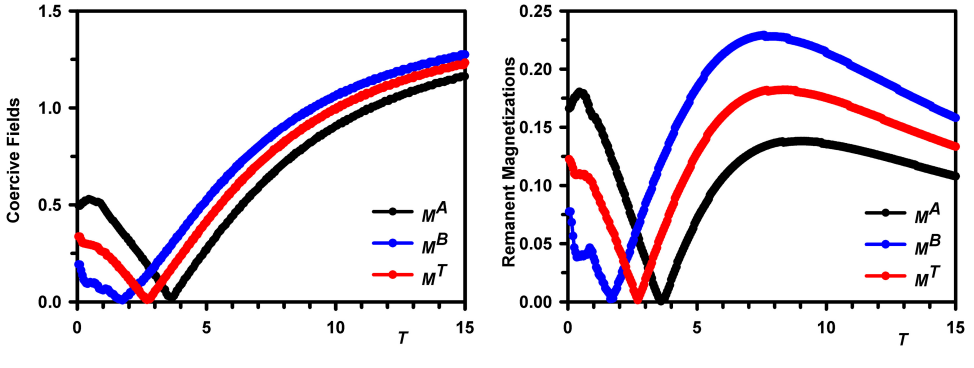


(b)

Fig. 4. (Color online) (a) The KMHLBs of m^A, m^B and m^T for fix $h_0 = 3.00$, $\omega = 6.00\pi$, $T = 0.50$, $k_1 = 1.0$, $d = 2.0$ but various rate constants (namely, wheel speed in rapid solidification techniques) k_2 values. (b) The behaviors of CFs and the RMs as a function of k_2.



(a)



(b)

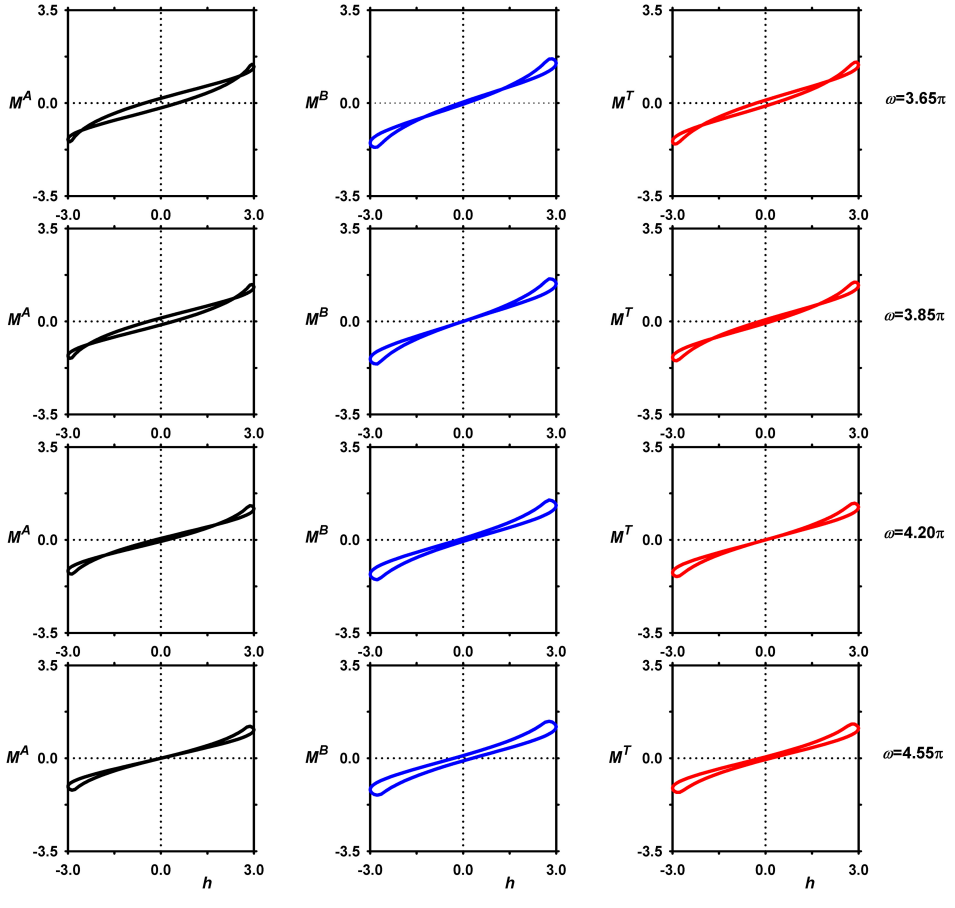
Fig. 5. (Color online) (a) The KMHLBs of m^A, m^B and m^T for fix $h_0 = 3.00$, $d = 2.0$, $\omega = 3.65\pi$, $k_1 = 1.0$, $k_2 = 2.0$, but various temperatures T values. (b) The behaviors of CFs and the RMs as a function of T.

hysteresis loop behaviors with such multiple loop areas, where the number of loops changes with increasing temperature and the elliptical loop areas become progressively narrower, have been reported in many theoretical studies on mixed-spin antiferrimagnetic Ising systems[41–51] and in experimental studies on magnetic materials.[52,53,58]

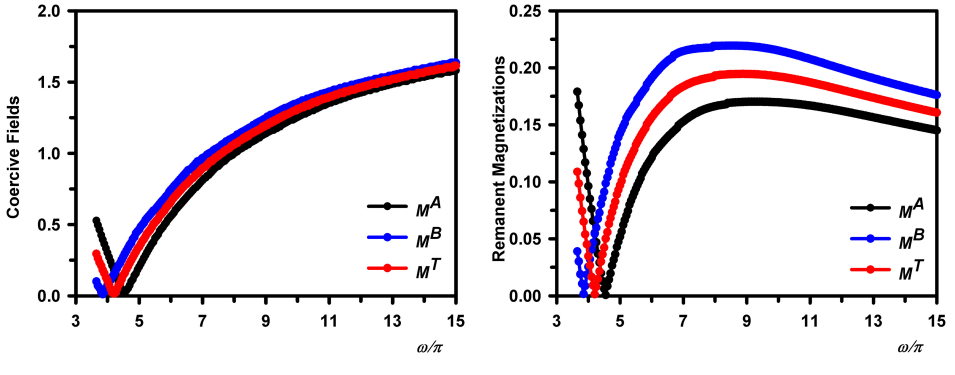
For d =2.0, $k_2 = 2.0$ and $T = 0.50$, the results obtained as a function of the oscillating frequency of the external magnetic field applied to the system are shown in Fig. 6. This figure proves that the kinetic magnetic hysteresis loop areas and the behaviors of CFs and RMs are surprisingly very similar to those in Fig. 5. However, this time the behavior is described with respect to increasing frequency. As the frequency increases, m^B first, then m^T, and subsequently m^A transform into narrow-area double loops. In all three cases, after the kinetic magnetic hysteresis loops convert to double loops, they exhibit a symmetric elliptical behavior with progressively narrowing areas. This kinetic magnetic hysteresis loop behavior is clearly seen from the CFs and RMs, which start at low temperatures and become zero at ω =3.85π, 4.20π and 4.55π for m^B, m^T and m^A, respectively, while CFs increase and RMs decrease thereafter. To the best of our knowledge, the kinetic magnetic hysteresis loop behaviors of different mixed-spin systems as a function of the external magnetic field's frequency have been investigated by very few research groups. In fact, many researchers have either not considered the external magnetic field at all or have assumed it to be constant. Therefore, for theoretical studies in this area, it is appropriate to reference the limited number of researchers, including our group, who perform calculations based on the frequency of a sinusoidal external magnetic field. In summary, the results of the current study as a function of frequency are in good agreement with theoretical studies on mixed-spin antiferrimagnetic Ising systems[44–51] and experimental studies,[58–61] except for the low sensitivity point of the kinetic hysteresis loops and their narrow loop areas.

Figure 7 shows the kinetic magnetic hysteresis loops for $k_2 = 2.0$, $\omega = 3.65\pi$ and $T = 0.50$ as a function of the reduced single-ion anisotropy parameter, d. Consistent with findings for other high-spin mixed-spin systems,[41–43] the parameter d does not significantly affect the behavior of the kinetic magnetic hysteresis loops. Specifically, for the given system parameters, the kinetic magnetic hysteresis loops for m^A, m^B and m^T exhibit a triple-loop character for low d values and maintain this triple-loop structure even when d is increased significantly. However, as shown in Fig. 7(b), the values of CFs and RMs show very little change at very small values of d and then show no change with increasing d.

Finally, Fig. 8 presents the kinetic magnetic hysteresis loops, as well as the CFs and RMs behaviors, as a function of the rate constant k_2, which is one of the advantages of PPM and corresponds to the wheel speed in rapid solidification techniques, for the system parameters $d = 2.0$, $\omega = 10.0\pi$ and $T = 1.00$. As stated in this subsection, all loop areas are narrow. At low k_2 values, the kinetic hysteresis loops for magnetizations m^A, m^B and m^T have a nearly rectangular structure with very narrow areas. When $k_2 = 3.00$, the kinetic hysteresis loop for m^A exhibits a

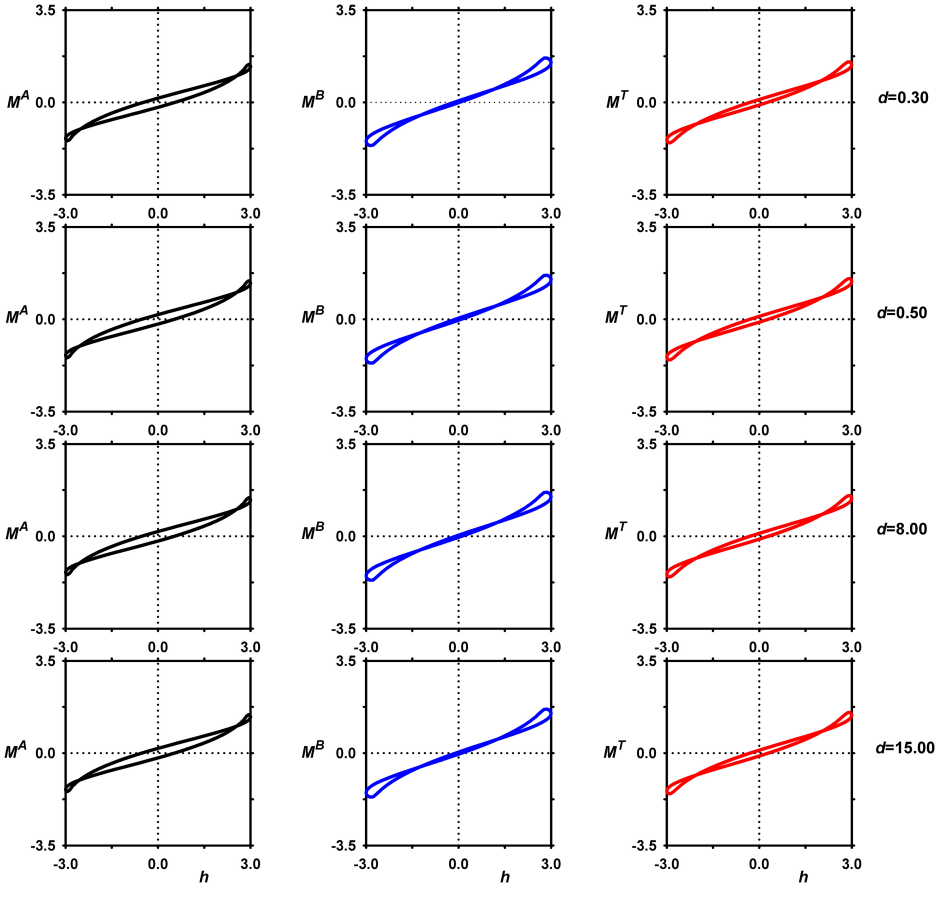


(a)

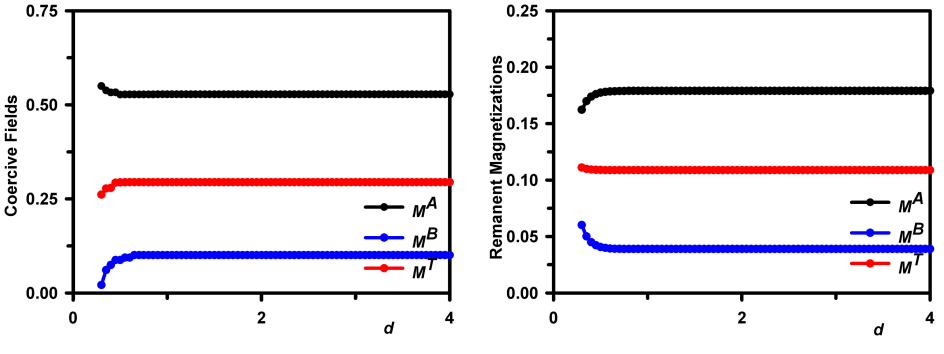


(b)

Fig. 6. (Color online) (a) The KMHLBs of m^A, m^B and m^T for fix $h_0 = 3.00$, $d = 2.0$, $T = 0.50$, $k_1 = 1.0$, $k_2 = 2.0$, but various frequencies of the oscillating field ω values. (b) The behaviors of CFs and the RMs as a function of ω.

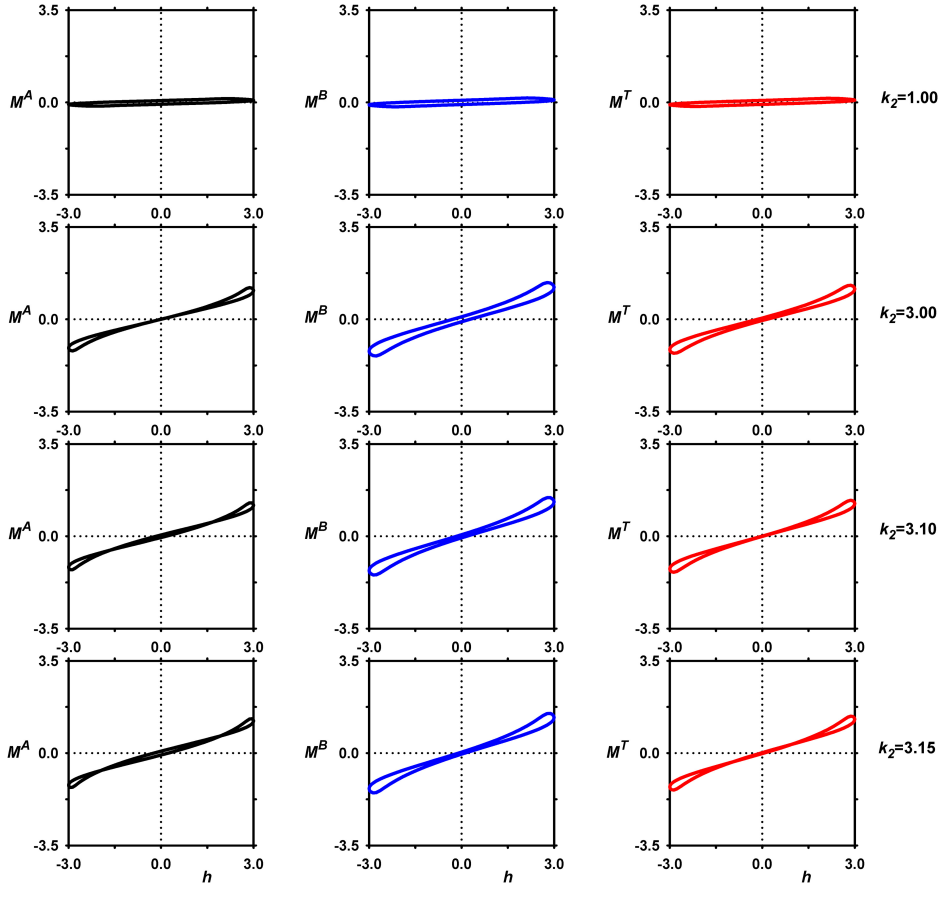


(a)

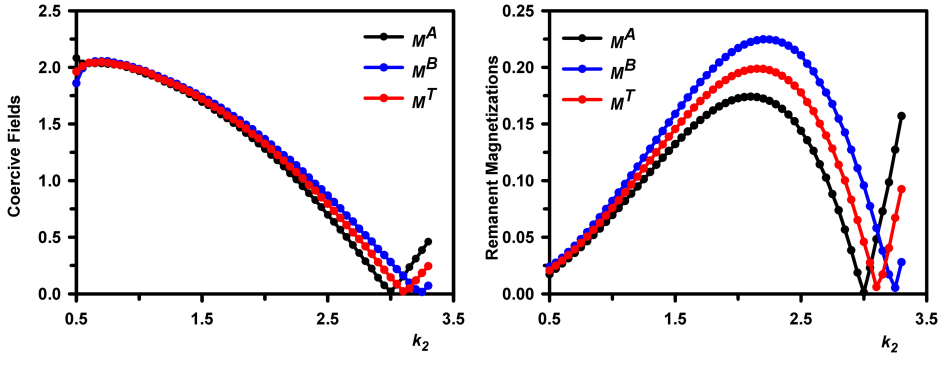


(b)

Fig. 7. (Color online) (a) The KMHLBs of m^A, m^B and m^T for fix $h_0 = 3.00$, $\omega = 3.65\pi$, $T = 0.50$, $k_1 = 1.0$, $k_2 = 2.0$, but various crystal-field interaction d values. (b) The behaviors of CFs and the RMs as a function of d.



(a)



(b)

Fig. 8. (Color online) (a) The DMHLBs of m^A, m^B and m^T for fix $h_0 = 3.00$, $\omega = 10.00\pi$, $T = 1.0$, $k_1 = 1.0$, but various rate constant (namely, wheel speed in rapid solidification techniques) k_2 values. (b) The behaviors of CFs and the RMs as a function of k_2.

double-loop character and evolves into a triple loop with increasing k_2. For m^T and m^B, there is no evolution to a triple loop with increasing k_2, but they first evolve into a double loop at $k_2 = 3.10$ and $k_2 = 3.15$, respectively. It should be noted that for the selected system parameters, there are no numerical solutions after $k_2 = 3.15$. It is obvious in Fig. 8(b) that the inversion points to the double loop are $k_2 = 3.0$, $k_2 = 3.10$ and $k_2 = 3.15$ for m^A, m^B and m^T, respectively. Multi-loops arise from phase-lagged sublattice reversals; higher k_2 strengthens the competition between driving and relaxation.

In the previously defined PPM, the k_1 parameter represented the translational motion of the spin particles, while the k_2 parameter, which corresponds to the wheel speed in the melt-spinning method, represented the rotational motion of the spin particles. In practice, $k_2 > k_1$ was assumed. Now, looking at the kinetic magnetic hysteresis loop behaviors obtained as a function of k_2, when $k_1 = k_2 = 1.0$, the loops for m^A, m^B and m^T are very narrow, and their saturation points are equal and close to zero. As k_2 is increased, in contrast to the ferrimagnetic state, multiple loops are observed for all three magnetizations, but the saturation points of the loops do not increase. However, the values of CFs gradually decrease from their large values, while the values of RMs increase from their low values. When they transition from a double-loop to a single-loop behavior, they become zero first, and then both CFs and RMs values tend to increase. Although the loop areas in the current system are very narrow, similar behaviors are in agreement with other theoretical studies.[41–52,56] As far as we know, the reason why we cannot observe these behaviors, especially the transitions between multiple loops, in experimental studies, is due to the inability to reach a sufficiently high wheel speed, which determines the strip thickness in the melt-spinning technique, and the concentration difference of the materials that make up the mixed-spin antiferrimagnetic material.[56]

For the antiferrimagnetic case ($J < 0$) and for rate constant values $k_2 = 3.15$, the numerical integration occasionally fails to converge because of multi-stability. This behavior originates from the coexistence of competing metastable branches in the kinetic regime, where rapid switching between local minima occurs when the effective relaxation outpaces the inter-sublattice coupling. Such nonconvergence reflects kinetic competition rather than a true mathematical singularity.

As a future extension, we will augment the deterministic PPM equations with Gaussian thermal noise to probe the robustness of multi-loop structures against stochastic perturbations.

4. Conclusion

In conclusion, this work provides an extensive analysis of the dynamic hysteresis in a mixed-spin (3, 7/2) BCIS, employing a time-dependent external magnetic field through the innovative PPM. The findings emphasize the importance of external magnetic field dynamics in affecting CFs and RM, distinguishing this study from prior research that primarily focused on static fields. Our results indicate that the interplay between temperature, crystal field, field frequency and kinetic constants

significantly influences the dynamic magnetic behaviors of molecular-based materials. This study therefore contributes to a deeper theoretical understanding of dynamic hysteresis phenomena in high-spin mixed-spin systems and provides a systematic framework for analyzing their kinetic magnetic behavior.

Such systems exhibiting tunable CFs, frequency-dependent loop areas and controllable RMs are directly related to the design of (i) magnetic field sensors and magnetoresistive detection elements, (ii) spintronic switching devices where controlled dynamic magnetization reversal is required, (iii) high-frequency magnetic recording media and (iv) molecular-based magnetic materials engineered for adjustable dynamic response. In particular, the dependence of the hysteresis loop area and CF on temperature, crystal-field interaction and external-field frequency provides guidance for optimizing dynamic performance in nanoscale magnetic systems. Similar connections between dynamic magnetic behavior and technological functionality have been discussed in Refs. 66–71.

Acknowledgments

This work was supported by the Erciyes University Research Funds (FBA-2025-14760). We thank the Editing Office of the Dean for Research at Erciyes University for editing and proofreading this paper.

Appendix A

Average dynamic equations for q^A, r^A, o^A, p^A, t^A and q^B, r^B, o^B, p^B, t^B, u^B.

$$\begin{aligned}\Omega\frac{dq^A}{d\xi} = &\left\{\left[(k_1-k_3)\left(\frac{19}{30}e^b\sinh(a)+\frac{13}{3}e^{4b}\sinh(2a)+\frac{21}{2}e^{9b}\sinh(3a)\right)\right]m^A\right.\\
&+\left[\left(-\frac{85}{36}k_1+\frac{13}{36}k_3\right)e^b\cosh(a)+\left(-\frac{58}{9}k_1+\frac{40}{9}k_3\right)e^{4b}\cosh(2a)\right.\\
&\left.+\left(-\frac{53}{4}k_1+\frac{45}{4}k_3\right)e^{9b}\cosh(3a)-2k_1\right]q^A\\
&+\left[(k_3-k_1)\left(\frac{2}{3}e^b\sinh(a)+\frac{17}{12}e^{4b}\sinh(2a)+\frac{8}{3}e^{9b}\sinh(3a)\right)\right]r^A\\
&+\left[(k_1-k_3)\left(\frac{7}{18}e^b\cosh(a)+\frac{14}{9}e^{4b}\cosh(2a)+\frac{7}{2}e^{9b}\cosh(3a)\right)\right]o^A\\
&+\left[(k_1-k_3)\left(\frac{1}{30}e^b\sinh(a)+\frac{1}{12}e^{4b}\sinh(2a)+\frac{1}{6}e^{9b}\sinh(3a)\right)\right]p^A\\
&+\left[(k_3-k_1)\left(\frac{1}{36}e^b\cosh(a)+\frac{1}{9}e^{4b}\cosh(2a)+\frac{1}{4}e^{9b}\cosh(3a)\right)\right]t^A\\
&\left.+2k_1(\cosh(a)e^b)+4\cosh(2a)e^{4b}+9\cosh(3a)e^{9b}\right\}\\
&/(k(1+2\cosh(a)e^b+2\cosh(2a)e^{4b}+2\cosh(3a)e^{9b}))\end{aligned} \tag{A.10b}$$

$$\Omega\frac{dr^A}{d\xi}=\Bigg\{\Bigg[\left(\frac{37}{30}k_1-3k_2+\frac{53}{30}k_3\right)e^b\cosh(a)+\left(\frac{148}{15}k_1+\frac{24}{5}k_2-\frac{44}{3}k_3\right)$$
$$\times e^{4b}\cosh(2a)+\left(\frac{333}{10}k_1-\frac{9}{5}k_2-\frac{63}{2}k_3\right)e^{9b}\cosh(3a)\Bigg]m^A$$
$$+\Bigg[\left(-\frac{187}{180}k_1+3k_2-\frac{187}{180}k_3\right)e^b\sinh(a)+\left(-\frac{517}{45}k_1-\frac{12}{5}k_2+\frac{125}{9}k_3\right)$$
$$\times e^{4b}\sinh(2a)+\left(-\frac{747}{20}k_1+\frac{3}{5}k_2+\frac{147}{4}k_3\right)e^{9b}\sinh(3a)\Bigg]q^A$$
$$+\Bigg[\left(-\frac{5}{4}k_1+\frac{13}{12}k_2-\frac{11}{6}k_3\right)e^b\cosh(a)+\left(-3k_1-\frac{16}{3}k_2+\frac{19}{3}k_3\right)$$
$$\times e^{4b}\cosh(2a)+\left(-\frac{31}{4}k_1+\frac{9}{4}k_2+\frac{7}{2}k_3\right)e^{9b}\cosh(3a)-2k_1\Bigg]r^A$$
$$+\Bigg[\left(-\frac{1}{36}k_1-\frac{13}{12}k_2+\frac{10}{9}k_3\right)e^b\sinh(a)+\left(\frac{97}{36}k_1+\frac{8}{3}k_2-\frac{193}{36}k_3\right)$$
$$\times e^{4b}\sinh(2a)+\left(\frac{121}{12}k_1-\frac{3}{4}k_2-\frac{28}{3}k_3\right)e^{9b}\sinh(3a)\Bigg]o^A$$
$$+\Bigg[\left(\frac{1}{60}k_1-\frac{1}{12}k_2+\frac{1}{15}k_3\right)e^b\cosh(a)+\left(\frac{2}{15}k_1+\frac{8}{15}k_2-\frac{2}{3}k_3\right)$$
$$\times e^{4b}\cosh(2a)+\frac{9}{20}(k_1-k_2)e^{9b}\cosh(3a)\Bigg]p^A$$
$$+\Bigg[\left(-\frac{1}{90}k_1+\frac{1}{12}k_2-\frac{13}{180}k_3\right)e^b\sinh(a)+\left(-\frac{37}{180}k_1-\frac{4}{15}k_2+\frac{17}{36}k_3\right)$$
$$\times e^{4b}\sinh(2a)+\left(-\frac{11}{15}k_1+\frac{3}{20}k_2+\frac{7}{12}k_3\right)e^{9b}\sinh(3a)\Bigg]t^A$$
$$+2k_1(\sinh(a)e^b)+8\sinh(2a)e^{4b}+27\sinh(3a)e^{9b}\Bigg\}$$
$$/(k(1+2\cosh(a)e^b+2\cosh(2a)e^{4b}+2\cosh(3a)e^{9b})) \tag{A.10c}$$

$$\Omega\frac{do^A}{d\xi}=\Bigg\{\Bigg[(k_1-k_3)\left(\frac{11}{6}e^b\sinh(a)+\frac{61}{3}e^{4b}\sinh(2a)+\frac{201}{2}e^{9b}\sinh(3a)\right)\Bigg]m^A$$
$$+\Bigg[(k_3-k_1)\left(\frac{49}{36}e^b\cosh(a)+\frac{196}{3}e^{4b}\cosh(2a)+\frac{144}{4}e^{9b}\cosh(3a)\right)\Bigg]q^A$$
$$+\Bigg[(k_3-k_1)\left(\frac{5}{3}e^b\sinh(a)+\frac{65}{12}e^{4b}\sinh(2a)+\frac{65}{3}e^{9b}\sinh(3a)\right)\Bigg]r^A$$
$$+\Bigg[\left(-\frac{11}{18}k_1-\frac{25}{18}k_3\right)e^b\cosh(a)+\left(\frac{47}{9}k_1-\frac{65}{9}k_3\right)e^{4b}\cosh(2a)$$
$$+\left(\frac{61}{2}k_1-\frac{54}{2}k_3\right)e^{9b}\cosh(3a)-2k_1\Bigg]o^A$$

$$
\begin{aligned}
&+\left[(k_1-k_3)\left(-\frac{1}{6}e^{b}\sinh(a)+\frac{1}{12}e^{4b}\sinh(2a)+\frac{7}{6}e^{9b}\sinh(3a)\right)\right]p^A\\
&+\left[(k_3-k_1)\left(\frac{1}{36}e^{b}\cosh(a)+\frac{4}{9}e^{4b}\cosh(2a)+\frac{9}{4}e^{9b}\cosh(3a)\right)\right]t^A\\
&+2k_1(\cosh(a)e^{b})+16\cosh(2a)e^{4b}+81\cosh(3a)e^{9b}\Bigg\}\\
&/(k(1+2\cosh(a)e^{b}+2\cosh(2a)e^{4b}+2\cosh(3a)e^{9b}))
\end{aligned}
\tag{A.10d}
$$

$$
\begin{aligned}
\Omega\frac{dp^A}{d\xi}=&\Bigg\{\Bigg[\left(\frac{37}{30}k_1-3k_2+\frac{53}{30}k_3\right)e^{b}\cosh(a)+\left(\frac{592}{15}k_1+\frac{96}{5}k_2-\frac{176}{3}k_3\right)\\
&\times e^{4b}\cosh(2a)+\left(\frac{2997}{10}k_1-\frac{81}{5}k_2-\frac{567}{2}k_3\right)e^{9b}\cosh(3a)\Bigg]m^A\\
&+\left[\left(-\frac{137}{180}k_1+3k_2-\frac{403}{180}k_3\right)e^{b}\sinh(a)+\left(-\frac{1933}{45}k_1-\frac{48}{5}k_2+\frac{473}{9}k_3\right)\right.\\
&\left.\times e^{4b}\sinh(2a)+\left(-\frac{6603}{20}k_1+\frac{27}{5}k_2+\frac{1299}{4}k_3\right)e^{9b}\sinh(3a)\right]q^A\\
&+\left[\left(-\frac{1}{4}k_1+\frac{13}{12}k_2-\frac{5}{6}k_3\right)e^{b}\cosh(a)+\left(-8k_1-\frac{64}{3}k_2+\frac{88}{3}k_3\right)\right.\\
&\left.\times e^{4b}\cosh(2a)+\left(-\frac{243}{4}k_1+\frac{81}{4}k_2+\frac{81}{2}k_3\right)e^{9b}\cosh(3a)\right]r^A\\
&+\left[\left(-\frac{37}{36}k_1-\frac{13}{12}k_2+\frac{19}{9}k_3\right)e^{b}\sinh(a)+\left(\frac{397}{36}k_1+\frac{32}{3}k_2-\frac{781}{36}k_3\right)\right.\\
&\left.\times e^{4b}\sinh(2a)+\left(\frac{1117}{12}k_1-\frac{27}{4}k_2-\frac{259}{3}k_3\right)e^{9b}\sinh(3a)\right]o^A\\
&+\Bigg[\left(-\frac{59}{60}k_1-\frac{1}{12}k_2-\frac{14}{15}k_3\right)e^{b}\cosh(a)+\left(-\frac{7}{15}k_1+\frac{32}{15}k_2-\frac{11}{3}k_3\right)\\
&\times e^{4b}\cosh(2a)+\left(\frac{61}{20}k_1-\frac{81}{20}k_2-k_3\right)e^{9b}\cosh(3a)-2k_1\Bigg]p^A\\
&+\left[\left(-\frac{19}{90}k_1+\frac{1}{12}k_2+\frac{23}{180}k_3\right)e^{b}\sinh(a)+\left(-\frac{193}{180}k_1-\frac{16}{15}k_2+\frac{77}{36}k_3\right)\right.\\
&\left.\times e^{4b}\sinh(2a)+\left(-\frac{104}{15}k_1+\frac{27}{20}k_2+\frac{67}{12}k_3\right)e^{9b}\sinh(3a)\right]t^A\\
&+2k_1(\sinh(a)e^{b}+32\sinh(2a)e^{4b}+243\sinh(3a)e^{9b}\Bigg\}\\
&/(k(1+2\cosh(a)e^{b}+2\cosh(2a)e^{4b}+2\cosh(3a)e^{9b}))
\end{aligned}
\tag{A.10e}
$$

$$\Omega\frac{dt^A}{d\xi}=\Bigg\{\Bigg[(k_1-k_3)\bigg(-\frac{151}{30}e^b\sinh(a)+\frac{217}{3}e^{4b}\sinh(2a)+\frac{1785}{2}e^{9b}\sinh(3a)\bigg)\Bigg]m^A$$
$$+\Bigg[(k_3-k_1)\bigg(\frac{49}{36}e^b\cosh(a)+\frac{784}{9}e^{4b}\cosh(2a)+\frac{3696}{4}e^{9b}\cosh(3a)\bigg]q^A$$
$$+\Bigg[(k_1-k_3)\bigg(\frac{28}{3}e^b\sinh(a)-\frac{77}{12}e^{4b}\sinh(2a)-\frac{518}{3}e^{9b}\sinh(3a)\bigg)\Bigg]r^A$$
$$+\Bigg[(k_1-k_3)\bigg(\frac{7}{18}e^b\cosh(a)+\frac{224}{9}e^{4b}\cosh(2a)+\frac{567}{2}e^{9b}\cosh(3a)\bigg]o^A$$
$$+\Bigg[(k_3-k_1)\bigg(\frac{119}{30}e^b\sinh(a)+\frac{35}{12}e^{4b}\sinh(2a)+\frac{49}{6}e^{9b}\sinh(3a)\bigg)\Bigg]p^A$$
$$+\Bigg[\bigg(-\frac{37}{36}k_1-\frac{35}{36}k_3\bigg)(e^b\cosh(a)+\bigg(-\frac{25}{9}k_1+\frac{7}{9}k_3\bigg)e^{4b}\cosh(2a)$$
$$+\bigg(-\frac{85}{5}k_1+\frac{77}{4}k_3\bigg)e^{9b}\cosh(3a))-2k_1\Bigg]t^A$$
$$+2k_1(\cosh(a)e^b+64\cosh(2a)e^{4b}+729\cosh(3a)e^{9b}\Bigg\}$$
$$/(k(1+2\cosh(a)e^b+2\cosh(2a)e^{4b}+2\cosh(3a)e^{9b})) \tag{A.10f}$$

and

$$\Omega\frac{dq^B}{d\xi}=\Bigg\{\Bigg[\bigg(\frac{1225}{2048}k_2+\frac{7621}{430080}k_1-\frac{7621}{430080}k_3\bigg)e^{b_4}\cosh(a_4)+(k_1+k_3)\frac{1225}{4096}$$
$$\times(e^{b_3}\cosh(a_3)+e^{b_2}\cosh(a_2)+e^{b_1}\cosh(a_1))+(k_1-k_3)$$
$$\bigg(\frac{29129}{143360}e^{b_4}\sinh(a_4)\ +\bigg(\frac{634149}{143360}e^{b_3}\sinh(a_3)\ +\bigg(\frac{1154915}{86016}e^{b_2}\sinh(a_2)$$
$$+\bigg(\frac{1654681}{61440}e^{b_1}\sinh(a_1)\bigg)\Bigg]m^B$$
$$+\Bigg[-\frac{16541}{18432}(k_1+k_3)(e^{b_4}\cosh(a_4)+e^{b_3}\cosh(a_3)+e^{b_2}\cosh(a_2)$$
$$+e^{b_1}\cosh(a_1)+\bigg(-\frac{1891}{18432}k_3+\frac{1891}{9216}k_2-\frac{1891}{18432}k_1\bigg)e^{b_4}\sinh(a_4)$$
$$+\frac{1891}{18432}(k_3-k_1)(e^{b_3}\sinh(a_3)+e^{b_2}\sinh(a_2)+e^{b_1}\sinh(a_1))\Bigg]q^B$$
$$+\Bigg[\bigg(\frac{229}{3072}k_3-\frac{1891}{4608}k_2-\frac{229}{3072}k_1\bigg)e^{b_4}\cosh(a_4)+-\frac{1891}{9216}(k_1+k_3)$$
$$\times(e^{b_3}\cosh(a_3)+e^{b_2}\cosh(a_2)+e^{b_1}\cosh(a_1))+\bigg(\frac{12839}{15360}k_3-\frac{1891}{9216}k_1\bigg)$$
$$\times e^{b_4}\sinh(a_4)\ +(k_3-k_1)\bigg(\frac{14313}{5120}e^{b_3}\sinh(a_3)+\frac{321457}{46080}e^{b_2}\sinh(a_2)$$

$$+\frac{610417}{46080}e^{b_1}\sinh(a_1)\Big)\Big]r^B+\Big[-\frac{83}{4608}(k_1+k_3)(e^{b_4}\cosh(a_4)$$
$$+e^{b_3}\cosh(a_3)+e^{b_2}\cosh(a_2)+e^{b_1}\cosh(a_1))+\Big(-\frac{83}{2304}k_2+\frac{83}{4608}k_1$$
$$+\frac{83}{4608}k_3\Big)e^{b_4}\sinh(a_4)\ +\frac{83}{4608}(k_1-k_3)(e^{b_3}\sinh(a_3)+e^{b_2}\sinh(a_2)$$
$$+e^{b_1}\sinh(a_1))]o^B+\Big[\Big(-\frac{19}{1280}k_3+\frac{19}{1280}k_1+\frac{83}{1152}k_2\Big)e^{b_4}\cosh(a_4)$$
$$+\frac{83}{2304}(k_1+k_3)(e^{b_3}\cosh(a_3)+e^{b_2}\cosh(a_2)+e^{b_1}\cosh(a_1))\ +(k_1-k_3)$$
$$\times\Big(\frac{359}{3840}e^{b_4}\sinh(a_4)+\frac{1579}{3840}e^{b_3}\sinh(a_3)+\frac{2509}{2304}e^{b_2}\sinh(a_2)$$
$$+\frac{24257}{11520}e^{b_1}\sinh(a_1)\Big)\Big]p^B+\Big[\frac{1}{1152}(k_1+k_3)(e^{b_4}\cosh(a_4)+e^{b_3}\cosh(a_3)$$
$$+e^{b_2}\cosh(a_2)+e^{b_1}\cosh(a_1))+\Big(-\frac{1}{1152}k_3+\frac{1}{576}k_2-\frac{1}{1152}k_1\Big)$$
$$\times e^{b_4}\sinh(a_4)+\frac{1}{1152}(k_3-k_1)(e^{b_3}\sinh(a_3)+e^{b_2}\sinh(a_2)+e^{b_1}\sinh(a_3))\Big]$$
$$\times t^B+\Big[\Big(\frac{1}{1344}k_3-\frac{1}{1344}k_1-\frac{1}{288}k_2\Big)e^{b_4}\cosh(a_4)-\frac{1}{576}(k_1+k_3)$$
$$\times(e^{b_3}\cosh(a_3)+e^{b_2}\cosh(a_2)+e^{b_1}\cosh(a_1))+(k_3-k_1)$$
$$\times\Big(\frac{127}{6720}e^{b_3}\sinh(a_3)+\frac{1021}{20160}e^{b_2}\sinh(a_2)+\frac{283}{2880}k_3e^{b_3}\sinh(a_3)\Big)\Big]u^B$$
$$+(k_1+k_3)\Big(\frac{1847}{8192}e^{b_4}\cosh(a_4)+\frac{17207}{8192}e^{b_3}\cosh(a_3)+\frac{17207}{8192}e^{b_2}\cosh(a_2)$$
$$+\frac{99127}{8192}e^{b_1}\cosh(a_1)\Big)+\Big(-\frac{1225}{4096}k_2+\frac{201}{8192}k_3+\frac{201}{8192}k_1\Big)e^{b_4}\sinh(a_4)$$
$$+\frac{1225}{8192}(k_1-k_3)(e^{b_3}\sinh(a_3)+e^{b_2}\sinh(a_2)+e^{b_1}\sinh(a_1))\Big\}$$
$$/(2k(\cosh(a_1)e^{b_1}+\cosh(a_2)e^{b_2}+\cosh(a_3)e^{b_3}+\cosh(a_4)e^{b_4}) \tag{A.11b}$$

$$\Omega\frac{dr^B}{d\xi}=\Big\{\Big[\Big(\frac{1225}{2048}k_2+\frac{30251}{107520}k_1+\frac{68123}{215040}k_3\Big)e^{b_4}\cosh(a_4)$$
$$+\Big(\frac{272259}{35840}k_1-\frac{621693}{71680}k_3+\frac{2205}{2048}k_2\Big)e^{b_3}\cosh(a_3)$$
$$+\Big(-\frac{1225}{2048}k_2-\frac{1486825}{43008}k_3+\frac{756275}{21504}k_1\Big)e^{b_2}\cosh(a_2)$$
$$+\Big(\frac{1482299}{15360}k_1-\frac{2968273}{30720}k_3+\frac{245}{2048}k_2\Big)e^{b_1}\cosh(a_1)\Big]m^B$$
$$+\Big[\Big(\frac{51037}{46080}k_3-\frac{1891}{9216}k_2-\frac{20791}{23040}k_1\Big)e^{b_4}\sinh(a_4)$$

$$
\begin{aligned}
&+\left(-\frac{54815}{9216}k_3-\frac{20791}{23040}k_1+\frac{35073}{5120}k_2\right)e^{b_3}\sinh(a_3)\\
&+\left(-\frac{20791}{23040}k_1+\frac{39273}{5120}k_3-\frac{62375}{9216}k_2\right)e^{b_2}\sinh(a_2)\\
&+\left(-\frac{9451}{9216}k_3+\frac{88837}{46080}k_2-\frac{20791}{23040}k_1\right)e^{b_1}\sinh(a_1)\Bigg]q^B\\
&+\Bigg[\left(\frac{5897}{4608}k_3+\frac{1891}{4608}k_2-\frac{2605}{2304}k_1\right)e^{b_4}\cosh(a_4)\\
&+\left(-\frac{11691}{2560}k_2-\frac{1159}{256}k_1+\frac{18161}{2560}k_3\right)e^{b_3}\cosh(a_3)\\
&+\left(\frac{12475}{4608}k_2+\frac{6463}{512}k_3-\frac{39929}{2304}k_1\right)e^{b_2}\cosh(a_2)\\
&+\left(\frac{12691}{23040}k_2+\frac{1022081}{23040}k_3-\frac{105547}{2304}k_1\right)e^{b_1}\cosh(a_1)\Bigg]r^B\\
&+\Bigg[\left(\frac{83}{2304}k_2-\frac{535}{1152}k_1+\frac{623}{2304}k_3\right)e^{b_4}\sinh(a_4)\\
&+\left(-\frac{353}{1152}k_1+\frac{4351}{2304}k_3-\frac{405}{256}k_2\right)e^{b_3}\sinh(a_3)\\
&+\left(-\frac{741}{256}k_3-\frac{353}{1152}k_1+\frac{7375}{2304}k_2\right)e^{b_2}\sinh(a_2)\\
&+\left(\frac{3107}{2304}k_3-\frac{353}{1152}k_1+\frac{2401}{2304}k_2\right)e^{b_1}\sinh(a_1)\Bigg]o^B\\
&+\Bigg[\left(\frac{293}{5760}k_3+\frac{61}{2880}k_1-\frac{83}{1152}k_2\right)e^{b_4}\cosh(a_4)\\
&+\left(\frac{135}{128}k_2-\frac{183}{320}k_1-\frac{1041}{640}k_3\right)e^{b_3}\cosh(a_3)\\
&+\left(-\frac{175}{128}k_3+\frac{1525}{576}k_1-\frac{1475}{1152}k_2\right)e^{b_2}\cosh(a_2)\\
&+\left(\frac{20923}{2880}k_1-\frac{43561}{5760}k_3+\frac{343}{1152}k_2\right)e^{b_1}\cosh(a_1)\Bigg]p^B\\
&+\Bigg[\left(\frac{11}{1440}k_1-\frac{17}{2880}k_3-\frac{1}{576}k_2\right)e^{b_4}\sinh(a_4)\\
&+\left(\frac{67}{320}k_3+\frac{11}{1440}k_1+\frac{125}{576}k_2\right)e^{b_2}\sinh(a_2)\\
&+\left(-\frac{73}{576}k_3+\frac{11}{1440}k_1+\frac{343}{2880}k_2\right)e^{b_1}\sinh(a_1)\Bigg]t^B\\
&+\Bigg[\left(-\frac{5}{2016}k_3-\frac{1}{1008}k_1+\frac{1}{288}k_2\right)e^{b_4}\cosh(a_4)\\
&+\left(-\frac{9}{160}k_2+\frac{93}{1220}k_3-\frac{3}{112}k_1\right)e^{b_3}\cosh(a_3)\\
&+\left(\frac{25}{672}k_3-\frac{125}{1008}k_1+\frac{25}{288}k_2\right)e^{b_2}\cosh(a_2)
\end{aligned}
$$

$$
\begin{aligned}
&+\left(-\frac{49}{144}k_1+\frac{539}{1440}k_3-\frac{49}{1440}k_2\right)e^{b_1}\cosh(a_1)\Big]u^B\\
&+\left(\frac{1225}{4096}k_2-\frac{1203}{4096}k_3+\frac{501}{2048}k_1\right)e^{b_4}\sinh(a_4)\\
&+\left(\frac{7157}{2048}k_1+\frac{19949}{4096}k_3-\frac{6615}{4096}k_2\right)e^{b_3}\sinh(a_3)\\
&+\left(\frac{32245}{2048}k_1+\frac{57385}{4096}k_3+\frac{6125}{4096}k_2\right)e^{b_2}\sinh(a_2)\\
&+\left(\frac{88053}{2048}k_1+\frac{176841}{4096}k_3-\frac{1715}{4096}k_2\right)e^{b_1}\sinh(a_1)\Big\}\\
&/(2k(\cosh(a_1)e^{b_1}+\cosh(a_2)e^{b_2}+\cosh(a_3)e^{b_3}+\cosh(a_4)e^{b_4}) \quad \text{(A.11c)}
\end{aligned}
$$

$$
\begin{aligned}
\Omega\frac{dp^B}{d\xi}=&\Big\{\Big[\left(-\frac{1225}{8192}k_2-\frac{14351881}{1720320}k_1-\frac{14336639}{1720320}k_3\right)e^{b_4}\cosh(a_4)\\
&+\left(\frac{4977029}{573440}k_1-\frac{16014769}{573440}k_3+\frac{19845}{8192}k_2\right)e^{b_3}\cosh(a_3)\\
&+\left(-\frac{84231}{4096}k_2-\frac{137276975}{114688}k_3+\frac{137705725}{114688}k_1\right)e^{b_2}\cosh(a_2)\\
&+\left(\frac{288463049}{245760}k_1-\frac{292958309}{245760}k_3+\frac{12005}{8192}k_2\right)e^{b_1}\cosh(a_1)\\
&+\frac{137837}{16384}(k_3-k_1)(e^{b_4}\sinh(a_4)+e^{b_3}\sinh(a_3)+e^{b_1}\sinh(a_1))\\
&-\frac{337489675}{344064}(k_3-k_1)e^{b_2}\sinh(a_2)\Big]m^B\\
&+\Big[\frac{7018435}{73728}(k_1+k_3)(e^{b_4}\cosh(a_4)+e^{b_3}\cosh(a_3)\\
&+e^{b_2}\cosh(a_2)+e^{b_1}\cosh(a_1))\\
&+\left(-\frac{11895223}{122880}k_3-\frac{1891}{36864}k_2+\frac{35704579}{368640}k_1\right)e^{b_4}\sinh(a_4)\\
&+\left(-\frac{8277281}{73728}k_3+\frac{35704579}{368640}k_1+\frac{315657}{20480}k_2\right)e^{b_3}\sinh(a_3)\\
&+\left(\frac{35704579}{368640}k_1+\frac{50073521}{368640}k_3-\frac{476545}{2048}k_2\right)e^{b_2}\sinh(a_2)\\
&+\left(-\frac{2960707}{24576}k_3+\frac{4353013}{184320}k_2+\frac{35704579}{368640}k_1\right)e^{b_1}\sinh(a_1)\Big]q^B\\
&+\Big[\left(\frac{1401109}{36864}k_3+\frac{1891}{18432}k_2+\frac{1402483}{36864}k_1\right)e^{b_4}\cosh(a_4)\\
&+\left(-\frac{105219}{10240}k_2+\frac{1111115}{36864}k_1+\frac{10375237}{184320}k_3\right)e^{b_3}\cosh(a_3)
\end{aligned}
$$

$$
\begin{aligned}
&+\left(\frac{95309}{1024}k_2+\frac{18669323}{36864}k_3-\frac{19293073}{36864}k_1\right)e^{b_2}\cosh(a_2)\\
&+\left(-\frac{621859}{92160}k_2+\frac{109440293}{184320}k_3-\frac{18831941}{36864}k_1\right)e^{b_1}\cosh(a_1)\\
&+\frac{1403687}{36864}(k_1-k_3)(e^{b_4}\sinh(a_4)+e^{b_3}\sinh(a_3)+e^{b_1}\sinh(a_1))\\
&+\frac{15530573}{36864}(k_3-k_1)e^{b_2}\sinh(a_2)\Big]r^B\\
&+\Big[-\frac{829835}{18432}(k_1+k_3)(e^{b_4}\cosh(a_4)\\
&+e^{b_3}\cosh(a_3)+e^{b_2}\cosh(a_2)+e^{b_1}\cosh(a_1))\\
&+\left(\frac{83}{9216}k_2-\frac{863839}{18432}k_1+\frac{287891}{6144}k_3\right)e^{b_4}\sinh(a_4)\\
&+\left(-\frac{863839}{18432}k_1+\frac{929449}{18432}k_3+\frac{3645}{1024}k_2\right)e^{b_3}\sinh(a_3)\\
&+\left(-\frac{1164581}{18432}k_3-\frac{863839}{18432}k_1+\frac{56345}{512}k_2\right)e^{b_2}\sinh(a_2)\\
&+\left(\frac{366379}{6144}k_3-\frac{863839}{18432}k_1-\frac{117649}{9216}k_2\right)e^{b_1}\sinh(a_1)\Big]o^B\\
&+\Big[\left(-\frac{875329}{46080}k_3-\frac{875671}{46080}k_1-\frac{83}{4608}k_2\right)e^{b_4}\cosh(a_4)\\
&+\left(\frac{1215}{512}k_2-\frac{816623}{46080}k_1-\frac{1044557}{46080}k_3\right)e^{b_3}\cosh(a_3)\\
&+\left(-\frac{608371}{9216}k_3+\frac{663689}{9216}k_1-\frac{11269}{256}k_2)e^{b_2}\cosh(a_2\right)\\
&+\left(\frac{3224993}{46080}k_1-\frac{5144893}{46080}k_3+\frac{16807}{4608}k_2\right)e^{b_1}\cosh(a_1)\\
&+\frac{165967}{9216}(k_3-k_1)(e^{b_4}\sinh(a_4)+e^{b_3}\sinh(a_3)\\
&+e^{b_2}\sinh(a_4)+e^{b_1}\sinh(a_1))]p^B\\
&+\Big[\frac{14065}{4608}(k_1+k_3)(e^{b_4}\cosh(a_4)+e^{b_3}\cosh(a_3)\\
&+e^{b_2}\cosh(a_2)+e^{b_1}\cosh(a_1))\\
&+\left(\frac{66961}{23040}k_1-\frac{7439}{2560}k_3-\frac{1}{2304}k_2\right)e^{b_4}\sinh(a_4)\\
&+\left(\frac{66961}{23040}k_1-\frac{14267}{4608}k_3+\frac{243}{1280}k_2\right)e^{b_3}\sinh(a_3)\\
&+\left(\frac{104939}{23040}k_3+\frac{66961}{23040}k_1-\frac{955}{128}k_2\right)e^{b_2}\sinh(a_2)\\
&+\left(-\frac{2235}{512}k_3+\frac{66961}{23040}k_1-\frac{16807}{11520}k_2\right)e^{b_1}\sinh(a_1)\Big]t^B\\
&+\Big[\left(\frac{19681}{16128}k_3+\frac{19687}{16128}k_1+\frac{1}{1152}k_2\right)e^{b_4}\cosh(a_4)
\end{aligned}
$$

$$
\begin{aligned}
&+\left(-\frac{81}{640}k_2+\frac{113521}{80640}k_3+\frac{18719}{16128}k_1\right)e^{b_3}\cosh(a_3)\\
&+\left(\frac{40319}{16128}k_3-\frac{49069}{16128}k_1+\frac{191}{64}k_2\right)e^{b_2}\cosh(a_2)\\
&+\left(-\frac{6791}{2304}k_1+\frac{66887}{11520}k_3-\frac{2401}{5760}k_2\right)e^{b_1}\cosh(a_1)\\
&+\frac{2813}{2304}(k_1-k_3)(e^{b_4}\sinh(a_4)+e^{b_3}\sinh(a_3)+e^{b_1}\sinh(a_1)\\
&+\frac{36569}{16128}(k_3-k_1)e^{b_2}\sinh(a_2))\Big]u^B\\
&-(k_1+k_3)\left(\frac{689185}{32768}(e^{b_4}\cosh(a_4)+e^{b_3}\cosh(a_3))\right.\\
&-\frac{13713375}{32768}e^{b_2}\cosh(a_2)+\frac{689185}{32768}e^{b_1}\cosh(a_1))\\
&+\left(\frac{1225}{16384}k_2+\frac{698539}{32768}k_3-\frac{698539}{32768}k_1\right)e^{b_4}\sinh(a_4)\\
&+\left(-\frac{451133}{32768}k_1+\frac{1067867}{32768}k_3-\frac{59535}{16384}k_2\right)e^{b_3}\sinh(a_3)\\
&+\left(\frac{16902595}{32768}k_1+\frac{16617305}{32768}k_3+\frac{421155}{8192}k_2\right)e^{b_2}\sinh(a_2)\\
&+\left.\left(\frac{16902595}{32768}k_1+\frac{18078403}{32768}k_3-\frac{84035}{16384}k_2\right)e^{b_1}\sinh(a_1)\right\}\\
&/(2k(\cosh(a_1)e^{b_1}+\cosh(a_2)e^{b_2}+\cosh(a_3)e^{b_3}+\cosh(a_4)e^{b_4})
\end{aligned}
\tag{A.11d}
$$

$$
\begin{aligned}
\Omega\frac{do^B}{d\xi}=&\left\{\left[(k_1-k_3)\left(\frac{6997}{8960}e^{b_4}\sinh(a_4)+\frac{103169}{8960}e^{b_3}\sinh(a_3)\right.\right.\right.\\
&\left.\left.\left.+\frac{473315}{5376}e^{b_2}\sinh(a_2)+\frac{1297471}{3840}e^{b_1}\sinh(a_1)\right)\right]m^B\\
&+\left[(k_3-k_1)\left(\frac{929}{960}e^{b_4}\sinh(a_4)+\frac{17837}{2880}e^{b_3}\sinh(a_3)\right.\right.\\
&\left.\left.+\frac{13353}{320}e^{b_2}\sinh(a_2)+\frac{151429}{320}e^{b_1}\sinh(a_1)\right)\right]r^B\\
&-\left[(k_1+k_3)(e^{b_4}\cosh(a_4)+e^{b_3}\cosh(a_3)\right.\\
&\left.+e^{b_2}\cosh(a_2)+e^{b_1}\cosh(a_1))\right]o^B\\
&+\left[(k_3-k_1)\left(\frac{71}{240}e^{b_4}\sinh(a_4)-\frac{397}{720}e^{b_3}\sinh(a_3)\right.\right.\\
&\left.\left.-\frac{101}{16}e^{b_2}\sinh(a_2)-\frac{6029}{240}e^{b_1}\sinh(a_1)\right)\right]p^B\\
&+\left[(k_3-k_1)\left(\frac{1}{140}e^{b_4}\sinh(a_4)+\frac{41}{1260}e^{b_3}\sinh(a_3)\right.\right.
\end{aligned}
$$

$$+\frac{127}{420}e^{b_2}\sinh(a_2)+\frac{71}{60}e^{b_1}\sinh(a_1)\Big)\Big]u^B$$
$$+(k_1+k_3)\Big(\frac{1}{16}e^{b_4}\cosh(a_4)+\frac{81}{16}e^{b_3}\cosh(a_3)$$
$$+\frac{625}{16}e^{b_2}\cosh(a_2)+\frac{2401}{16}e^{b_1}\cosh(a_1)\Big)\Big\}$$
$$/(k(2\cosh(a_1)e^{b_1}+2\cosh(a_2)e^{b_2}$$
$$+2\cosh(a_3)e^{b_3}+2\cosh(a_4)e^{b_4})) \tag{A.11e}$$

$$\Omega\frac{dt^B}{d\xi}=\Big\{\Big[\Big(\frac{63181}{215040}(k_3-k_1)e^{b_4}\sinh(a_4)+\frac{1814167}{71680}(k_1-k_3)$$
$$\times e^{b_3}\sinh(a_3)+\frac{23619445}{43008}(k_1-k_3)e^{b_2}\sinh(a_2)\Big).$$
$$+\frac{127097033}{30720}(k_1-k_3)e^{b_1}\sinh(a_1)\Big]m^B$$
$$+\Big[\frac{4211}{2560}(k_1-k_3)e^{b_4}\sinh(a_4)-\frac{236011}{23040}(k_1-k_3)e^{b_3}\sinh(a_3)$$
$$+\frac{648959}{2560}(k_3-k_1)e^{b_2}\sinh(a_2)$$
$$+\frac{4914129}{2560}(k_3-k_1)e^{b_1}\sinh(a_1)\Big]r^B$$
$$+\Big[\frac{1179}{640}(k_3-k_1)e^{b_4}\sinh(a_4)+\frac{491}{5760}(k_1-k_3)e^{b_3}\sinh(a_3)$$
$$+\frac{5059}{128}(k_1-k_3)e^{b_2}\sinh(a_2)$$
$$+\frac{198169}{640}(k_1-k_3)e^{b_1}\sinh(a_1)\Big]p^B$$
$$-(k_1+k_3)[e^{b_4}\cosh(a_4)+e^{b_3}\cosh(a_3)$$
$$+e^{b_2}\cosh(a_2)+e^{b_1}\cosh(a_1)]t^B$$
$$+(k_3-k_1)\Big[\frac{491}{3360}e^{b_4}\sinh(a_4)+\frac{2383}{10080}e^{b_3}\sinh(a_3)$$
$$+\frac{7001}{3360}e^{b_2}\sinh(a_2)-\frac{7073}{480}e^{b_1}\sinh(a_1)\Big]u^B$$
$$+(k_1+k_3)\Big(\frac{1}{64}e^{b_4}\cosh(a_4)+\frac{15625}{64}e^{b_2}\cosh(a_2)$$
$$+\frac{117649}{64}e^{b_1}\cosh(a_1)\Big)\Big\}$$
$$/(2k(\cosh(a_1)e^{b_1}+\cosh(a_2)e^{b_2}$$
$$+\cosh(a_3)e^{b_3}+\cosh(a_4)e^{b_4}) \tag{A.11f}$$

$$\Omega\frac{du^B}{d\xi}=\Bigg\{\Bigg[\Bigg(-\frac{1225}{32768}k_2+\frac{1120327917}{215613440}k_1+\frac{3362416499}{646840320}k_3\Bigg)e^{b_4}\cosh(a_4)$$
$$+\Bigg(\frac{28225369687}{646840320}k_1-\frac{25051813637}{646840320}k_3$$
$$+\frac{178605}{32768}k_2)e^{b_3}\cosh(a_3)$$
$$+\Bigg(-\frac{120203125}{9240576}k_2-\frac{289779640625}{388104192}k_3$$
$$+\frac{298847703125}{388104192}k_1\Bigg)e^{b_2}\cosh(a_2)$$
$$+\Bigg(\frac{446220825883}{30801920}k_1-\frac{1339364297299}{92405760}k_3+\frac{588245}{32768}k_2\Bigg)$$
$$\times e^{b_1}\cosh(a_1)+(k_1+k_3)\Bigg(\frac{95703125}{18481152}e^{b_4}\sinh(a_4)$$
$$+\frac{95703125}{18481152}e^{b_3}\sinh(a_3)-\frac{234326171875}{388104192}e^{b_2}\sinh(a_2)$$
$$+\frac{95703125}{18481152}e^{b_1}\sinh(a_1)\Bigg)\Bigg]m^B$$
$$+\Bigg[(k_1+k_3)\Bigg(\frac{4873046875}{83165184}e^{b_4}\cosh(a_4)+\frac{4873046875}{83165184}e^{b_3}\cosh(a_3)$$
$$+\frac{4873046875}{83165184}e^{b_2}\cosh(a_2)$$
$$+\frac{4873046875}{83165184}e^{b_1}\cosh(a_1)\Bigg)+\Bigg(\frac{36760102763}{415825920}k_3-\frac{1891}{147456}k_2$$
$$-\frac{36754770143}{415825920}k_1\Bigg)e^{b_4}\sinh(a_4)+\Bigg(\frac{4466859151}{83165184}k_3$$
$$-\frac{36754770143}{415825920}k_1-\frac{2840913}{81920}k_2\Bigg)e^{b_3}\sinh(a_3)$$
$$+\Bigg(-\frac{36754770143}{415825920}k_1+\frac{97960238893}{415825920}k_3-\frac{6120546875}{41582592}k_2\Bigg)e^{b_2}\sinh(a_2)$$
$$+\Bigg(-\frac{16709019425}{83165184}k_3+\frac{213297637}{737280}k_2-\frac{36754770143}{415825920}k_1\Bigg)e^{b_1}\sinh(a_1)\Bigg]q^B$$
$$+\Bigg[\Bigg(-\frac{975336371}{41582592}k_3+\frac{1891}{73728}k_2-\frac{974948903}{41582592}k_1\Bigg)$$
$$\times e^{b_4}\cosh(a_4)+\Bigg(-\frac{946971}{40960}k_2-\frac{1717157111}{41582592}k_1$$
$$+\frac{366516601}{207912960}k_3\Bigg)e^{b_3}\cosh(a_3)$$
$$+\Bigg(\frac{1224109375}{20791296}k_2+\frac{11344984375}{41582592}k_3-\frac{15742421875}{41582592}k_1\Bigg)$$
$$\times e^{b_2}\cosh(a_2)+\Bigg(\frac{30471091}{368640}k_2$$

$$+\frac{1410392186969}{207912960}k_3-\frac{280590517079}{41582592}k_1\Big)$$
$$\times e^{b_1}\cosh(a_1)+\frac{974609375}{41582592}(k_1-k_3)(e^{b_4}\sinh(a_4)+e^{b_3}\sinh(a_3)$$
$$+e^{b_1}\sinh(a_1))-\frac{10783203125}{41582592}(k_1-k_3)e^{b_2}\sinh(a_2)\Big]r^B$$
$$+\Big[-\frac{576171875}{20791296}(k_1+k_3)(e^{b_4}\cosh(a_4)+e^{b_3}\cosh(a_3)$$
$$+e^{b_2}\cosh(a_2)+e^{b_1}\cosh(a_1))$$
$$+\Big(\frac{83}{36864}k_2+\frac{985237691}{20791296}k_1-\frac{985237691}{20791296}k_3\Big)$$
$$\times e^{b_4}\sinh(a_4)+\Big(\frac{985237691}{20791296}k_1-\frac{818719511}{20791296}k_3-\frac{32805}{4096}k_2\Big)$$
$$\times e^{b_3}\sinh(a_3)+\Big(-\frac{2432581441}{20791296}k_3+\frac{985237691}{20791296}k_1$$
$$+\frac{723671875}{10395648}k_2\Big)e^{b_2}\sinh(a_2)$$
$$+\Big(\frac{2266110073}{20791296}k_3+\frac{985237691}{20791296}k_1$$
$$-\frac{5764801}{36864}k_2\Big)e^{b_1}\sinh(a_1)\Big]o^B$$
$$+\Big[\Big(\frac{576337127}{51978240}k_3+\frac{576337127}{51978240}k_1-\frac{83}{18432}k_2\Big)$$
$$\times e^{b_4}\cosh(a_4)+\Big(\frac{10935}{2048}k_2+\frac{726654971}{51978240}k_1$$
$$+\frac{148158479}{51978240}k_3\Big)e^{b_3}\cosh(a_3)$$
$$+\Big(-\frac{193859375}{10395648}k_3+\frac{713796875}{10395648}k_1-\frac{144734375}{5197824}k_2\Big)$$
$$\times e^{b_2}\cosh(a_2)+\Big(\frac{57242518619}{51978240}k_1-\frac{58412566129}{51978240}k_3$$
$$+\frac{823543}{18432}k_2\Big)e^{b_1}\cosh(a_1)$$
$$+\Big(\frac{115234375}{10395648}k_3-\frac{115234375}{10395648}k_1\Big)e^{b_4}\sinh(a_4)$$
$$+\Big(\frac{115234375}{10395648}k_3-\frac{115234375}{10395648}k_1\Big)e^{b_3}\sinh(a_3)$$
$$+\Big(-\frac{361328125}{10395648}k_3+\frac{361328125}{10395648}k_1\Big)e^{b_2}\sinh(a_2)$$
$$+\Big(-\frac{115234375}{10395648}k_3-\frac{115234375}{10395648}k_1\Big)e^{b_1}\sinh(a_1)\Big]p^B$$

$$
\begin{aligned}
&+\Bigg[\frac{9765625}{5197824}(k_1+k_3)(e^{b_4}\cosh(a_4)\\
&+e^{b_3}\cosh(a_3)+e^{b_2}\cosh(a_2)+e^{b_1}\cosh(a_1))\\
&+\left(-\frac{176460197}{25989120}k_1+\frac{176460197}{25989120}k_3-\frac{1}{9216}k_2\right)e^{b_4}\sinh(a_4)\\
&+\left(-\frac{176460197}{25989120}k_1+\frac{33071797}{5197824}k_3+\frac{2187}{5120}k_2\right)e^{b_3}\sinh(a_3)\\
&+\left(\frac{299116447}{25989120}k_3-\frac{176460197}{25989120}k_1-\frac{12265625}{2598912}k_2\right)e^{b_2}\sinh(a_2)\\
&+\left(-\frac{57603611}{5197824}k_3-\frac{176460197}{25989120}k_1+\frac{823543}{46080}k_2\right)e^{b_1}\sinh(a_1)\Bigg]t^B\\
&+\left(-\frac{31867079}{18192384}k_3-\frac{31865387}{18192384}k_1+\frac{1}{4608}k_2\right)e^{b_4}\cosh(a_4)\\
&+\left(-\frac{729}{2560}k_2-\frac{121083787}{90961920}k_3-\frac{34331195}{18192384}k_1\right)e^{b_3}\cosh(a_3)\\
&+\left(-\frac{17145509}{18192384}k_3-\frac{80926759}{18192384}k_1+\frac{2453125}{1299456}k_2\right)e^{b_2}\cosh(a_2)\\
&+\left(-\frac{137260109}{2598912}k_1+\frac{707134211}{12994560}k_3-\frac{117649}{23040}k_2\right)e^{b_1}\cosh(a_1)\\
&+\frac{1953125}{2598912}(k_1-k_3)(e^{b_4}\sinh(a_4)+e^{b_3}\sinh(a_3)\\
&+e^{b_1}\sinh(a_1)+\frac{25390625}{18192384}(k_1-k_3)e^{b_2}\sinh(a_2)\Bigg]u^B\\
&+\frac{478515625}{36962304}(k_3-k_1)(e^{b_4}\cosh(a_4)+e^{b_3}\cosh(a_3)\\
&+e^{b_1}\cosh(a_1))+\frac{3173828125}{12320768}(k_1+k_3)e^{b_2}\cosh(a_2)\\
&+\left(\frac{1225}{65536}k_2-\frac{711336517}{36962304}k_3+\frac{711223153}{36962304}k_1\right)e^{b_4}\sinh(a_4)\\
&+\left(\frac{1342470001}{36962304}k_1+\frac{222800891}{36962304}k_3-\frac{535815}{65536}k_2\right)e^{b_3}\sinh(a_3)\\
&+\left(\frac{4423644795}{12320768}k_1+\frac{3549011455}{12320768}k_3+\frac{601015625}{18481152}k_2\right)e^{b_2}\sinh(a_2)\\
&+\Bigg(\frac{238523799409}{36962303}k_1+\frac{238523799409}{36962303}k_3\\
&-\frac{4117715}{65536}k_2\Bigg)e^{b_1}\sinh(a_1)\Bigg\}\\
&/(2k(\cosh(a_1)e^{b_1}+\cosh(a_2)e^{b_2}\\
&+\cosh(a_3)e^{b_3}+\cosh(a_4)e^{b_4}) \qquad \text{(A.11g)}
\end{aligned}
$$

where $a=(Jm^B+h)/T,\ b=d/T,\ c=(Jm^A+h)/T,\ a_1=\frac{7}{2}c,\ a_2=\frac{5}{2}c,\ a_3=\frac{3}{2}c,$ $a_4=\frac{1}{2}c,\ b_1=\frac{49}{4}b,\ b_2=\frac{25}{4}b,\ b_3=\frac{9}{4}b,\ b_4=\frac{1}{4}b,\ h=H/z,\ d=D/z,\ T=(\beta z)^{-1},\ z=4$ and $\Omega=\omega/k,\ k=k_1/k_2,\ k_3=\sqrt{k_1k_2},\ \xi=\omega t.$

ORCID

Mustafa Gençaslan https://orcid.org/0000-0002-5726-1733
Ahmet Dervişoğlu https://orcid.org/0000-0003-1593-1724

References

1. O. Kahn, *Molecular Magnetism* (VCH Publishers, New York, 1993).
2. J. S. Miller and A. J. Epstein, *MRS Bull.* **25**, 21 (2000).
3. D. Gatteschi, R. Sessoli and J. Villain, *Molecular Magnetism* (Oxford University Press, New York, 2006).
4. E. Coronado *et al.*, *Nature* **408**, 447 (2000).
5. L. Bogani and W. Wernsdorfer, *Nat. Mater.* **7**, 179 (2008).
6. L. Néel, *Ann. Phys.* **3**, 137 (1948).
7. G. Bertotti, *Hysteresis in Magnetism: For Physicists, Materials Scientists, and Engineers* (Academic Press, 1998).
8. M. Ertas, M. Keskin and B. Deviren, *J. Stat. Phys.* **146**, 1244 (2012).
9. H. K. Mohamad, *J. Magn. Magn. Mater.* **323**, 61 (2011).
10. F. Abubrig, *Open J. Appl. Sci.* **3**, 270 (2013).
11. U. Temizer, *J. Supercond. Nov. Magn.* **31**, 889 (2018).
12. S. Sabri, M. El Falaka, M. El Yadari, A. Benyoussef and A. El Kenz, *Physica A* **460**, 210 (2016).
13. B. Deviren, S. Akbudak and M. Keskin, *Solid State Commun.* **151**, 193 (2010).
14. K. Htoutou, Y. Benhouria, A. Oubelkacem, R. Ahl Laamara and L. B. Drissi, *Chin. Phys. B* **26**, 127501 (2017).
15. K. Htoutou, A. Oubelkacem, Y. Benhouria, I. Essaoudi, A. Ainane and R. Ahuja, *J. Supercond. Nov. Magn.* **30**, 1247 (2017).
16. W. Wang, D. Lv, Y. Liu, Y. Yang, Z.-Y. Gao and X.-R. Zhao, *Superlattices Microstruct.* **112**, 688 (2017).
17. A. Jabar, R. Masrour, A. Benyoussef and M. Hamedoun, *Chem. Phys. Lett.* **670**, 16 (2017).
18. C. H. N. Motlagh and G. Rezaei, *J. Magn. Magn. Mater.* **445**, 26 (2018).
19. D. Z. Fadil, M. Qajjour, A. Mhirech, B. Kabouchi, L. Bahmad and W. Ousi Benomar, *J. Magn. Magn. Mater.* **491**, 165559 (2019).
20. B. Boughazi, M. Boughrara and M. Kerouad, *Chin. Phys. B* **28**, 027501 (2019).
21. H. M. Yang, W. Wang, B.-C. Li, H.-J. Wu, S.-Q. Yang and J. Yang, *Physica A* **539**, 122932 (2020).
22. R. Bouachraoui, Y. Ziat, Y. Sbai, O. Rhazouani, F. Goumrhar and L. Bahmad, *J. Alloys Compd.* **809**, 151785 (2019).
23. T. Sahdane, S. Mtougui, F. Goumrhar, N. Mamouni, E. Salmani, H. Ez-Zahraouy, A. Benyoussef and O. Mounkachi, *Philos. Mag.* **101**, 1836 (2021).
24. R. Kikuchi, *Phys. Rev.* **81**, 988 (1951); R. Kikuchi, *Suppl. Prog. Theor. Phys.* **35**, 1 (1966).
25. D. Turnbull, in *Rapid Solidification Technology*, ed. R. L. Ashbrook (American Society for Metals, Metals Park, OH, 1983).
26. H. Jones, *Rapid Solidification of Metals and Alloys* (Institute of Metallurgists, London, 1982).
27. E. Karaköse and M. Keskin, *J. Alloys Compd.* **619**, 82 (2015).
28. E. Karaköse, A. İbrahim and M. Keskin, *J. Inorg. Organomet. Polym. Mater.* **28**, 2645 (2018).

29. M. Arejdal, A. Jabar, L. Bahmad and A. Benyoussef, *J. Supercond. Nov. Magn.* **29**, 2553 (2016).
30. M. Arejdal, L. Bahmad and A. Benyoussef, *Physica B* **504**, 116 (2017).
31. R. Masrour and A. Jabar, *J. Magn. Magn. Mater.* **426**, 225 (2017).
32. H. Bouda, L. Bahmad, R. Masrour and A. Benyoussef, *J. Supercond. Nov. Magn.* **32**, 1837 (2019).
33. A. A. Abed and H. K. Mohamad, *Solid State Commun.* **338**, 114456 (2021).
34. A. A. Abed and H. K. Mohamad, *AIP Conf. Proc.* **2398**, 020070 (2022).
35. M. Karimou, G. D. Ngantso, C. M. Salgado and A. S. de Arruda, *Chin. J. Phys.* **88**, 879 (2024).
36. Z. D. Vatansever, E. Vatansever, A. Berger, A. Vasilopoulos and N. Fytas, *Phys. Rev. E* **110**, 064155 (2024).
37. M. Batı, *Eur. Phys. J. B* **98**, 194 (2025).
38. Ü. Temizer, *Bozok J. Sci.* **3**, 34 (2025).
39. M. Chen, X. H. Zhao and Y.-H. Ma, preprint, doi:10.48550/arXiv.2506.24035.
40. N. Paran and M. Ertaş, *Phys. Status Solidi B* **262**, 2500042 (2025).
41. M. Gençaslan, M. F. I. Alhameri and A. Dervişoğlu, *J. Supercond. Nov. Magn.* **38**, 256 (2025).
42. M. Gençaslan and M. F. I. Alhameri, *Int. J. Mod. Phys. B* **40**, 2650051 (2026).
43. M. Gençaslan and B. Taş, *J. Magn. Magn. Mater.* **645**, 173958 (2026).
44. M. Gençaslan and M. Keskin, *J. Magn. Magn. Mater.* **514**, 167242 (2020).
45. M. Ertaş and M. Keskin, *Physica A* **526**, 120933 (2019).
46. K. Chakrabarti and M. Acharyya, *Rev. Mod. Phys.* **71**, 847 (1999).
47. M. Keskin and M. Ertaş, *Phys. Scr.* **95**, 055805 (2020).
48. M. Batı and M. Ertaş, *Physica B* **513**, 40 (2017).
49. M. Gençaslan and M. Keskin, *Int. J. Mod. Phys. B* **35**, 2150217 (2021).
50. M. Batı and M. Ertaş, *Phase Transit.* **90**, 863 (2017).
51. M. Keskin and M. Ertaş, *J. Supercond. Nov. Magn.* **30**, 3439 (2017).
52. M. Prester *et al.*, *Phys. Rev. B* **84**, 064441 (2011).
53. M. Dalal *et al.*, *J. Phys.: Condens. Matter* **29**, 085803 (2017).
54. M. Batı and M. Ertaş, *J. Supercond. Nov. Magn.* **29**, 2835 (2016).
55. M. Ertaş and M. Keskin, *Phys. Lett. A* **379**, 1576 (2015).
56. M. Gençaslan and A. M. Kaif Awwadee, *J. Supercond. Nov. Magn.* **37**, 1105 (2024).
57. M. Gençaslan and M. Keskin, *Phase Transit.* **95**, 372 (2022).
58. Y. L. He and G. C. Wang, *Phys. Rev. Lett.* **70**, 2336 (1993).
59. J. S. Suen and J. L. Erskine, *Phys. Rev. Lett.* **78**, 3567 (1997).
60. J. S. Suen *et al.*, *Phys. Rev. B* **59**, 4249 (1999).
61. T. A. Moore *et al.*, *J. Appl. Phys.* **89**, 7018 (2001).
62. S. S. Makridis and W. Tang, *J. Rare Earths* **30**, 691 (2012).
63. W. J. Yao *et al.*, *Mater. Sci. Eng. B* **178**, 752 (2013).
64. K. Umadevi *et al.*, *J. Supercond. Nov. Magn.* **29**, 2455 (2016).
65. S. Öztürk *et al.*, *Int. J. Mater. Sci. Appl.* **6**, 241 (2017).
66. E. Dagotto, *Science* **309**, 257 (2005).
67. E. D. T. De Lacheisserie, D. Gignoux and M. Schlenker (eds.), *Magnetism: II — Materials and Applications* (Springer, 2012).
68. S. A. Wolf *et al.*, *Science* **294**, 488 (2001).
69. D. J. Craik, *Magnetism: Principles and Applications* (Wiley, 1995).
70. M. Bibes and A. Barthélémy, *Nat. Mater.* **7**, 425 (2008).
71. R. C. O'Handley, *Modern Magnetic Materials: Principles and Applications* (Wiley, 2000).